NASA

National
Aeronautics and
Space
Administration

CR-179507
OCTOBER 20, 1986
21-5988

R-0

THERMAL BARRIER COATING LIFE-PREDICTION MODEL DEVELOPMENT

SECOND ANNUAL REPORT

BY

T.E. STRANGMAN

J. NEUMANN

A. LIU

FOR NASA LERC CONTRACT NAS3-23945

GARRETT TURBINE ENGINE COMPANY
A DIVISION OF THE GARRETT CORPORATION
PHOENIX, ARIZONA

1. Report No.	2. Government Accession No.	3. Recipient's Catalog No.
CR-179507		

4. Title and Subtitle	5. Report Date
Thermal Barrier Coating Life-Prediction Model Development Annual Report	October 20, 1986
	6. Performing Organization Code

7. Author(s)	8. Performing Organization Report No.
T.E. Strangman J. Neumann A. Liu	21-5988
	10. Work Unit No.

9. Performing Organization Name and Address	11. Contract or Grant No.
Garrett Turbine Engine Company 111 S. 34th Street, P.O. Box 5217 Phoenix, AZ 85010	NAS3-23945
	13. Type of Report and Period Covered

12. Sponsoring Agency Name and Address	13. Type of Report and Period Covered
NASA-Lewis Research Center	Annual, Second Year
	14. Sponsoring Agency Code

15. Supplementary Notes

Project Manager: R.A. Miller
NASA-Lewis Research Center
Cleveland, Ohio 44135

16. Abstract

This report contains preliminary information and shall be considered as an informal document.

This program focuses on predicting the lives of two types of strain-tolerant and oxidation-resistant TBC systems that are produced by commercial coating suppliers to the gas turbine industry. The plasma-sprayed TBC system, composed of a low-pressure plasma-spray (LPPS) or an argon shrouded plasma-spray (ASPS) applied oxidation resistant NiCrAlY (or CoNiCrAlY) bond coating and an air-plasma-sprayed yttria (8 percent) partially stabilized zirconia insulative layer, is applied by both Chromalloy (Orangeburg, New York), Klock (Manchester, Connecticut) and Union Carbide (Indianapolis, Indiana). The second type of TBC is applied by the electron beam - physical vapor deposition (EB-PVD) process by Temescal (Berkeley, California).

The second year of this multiyear program was focused on specimen procurement, TBC system characterization, nondestructive evaluation methods, life prediction model development, and TFE731 engine testing of thermal barrier coated blades.

Materials testing is approaching completion. Thermomechanical characterization of the TBC systems, with toughness, and spalling strain tests, has been completed. Modulus testing is in progress. Thermochemical testing is approximately two-thirds complete. Preliminary materials life models for the bond coating oxidation and zirconia sintering failure modes have been developed. Integration of these life models with airfoil component analysis methods is in progress. Testing of high pressure turbine blades coated with the program TBC systems is in progress in a TFE731 turbofan engine.

Eddy current technology feasibility has been established with respect to nondestructively measuring zirconia layer thickness of a TBC system. Testing of high pressure turbine blades coated with the program TBC systems is in progress in a TFE731 turbofan engine.

17. Key Words (Suggested by Author(s))	18. Distribution Statement
Thermal Barrier Life Prediction Development Program	

19. Security Classif. (of this report)	20. Security Classif. (of this page)	21. No. of Pages	22. Price*
UNCLASSIFIED	UNCLASSIFIED	84	

* For sale by the National Technical Information Service, Springfield, Virginia 22161

TABLE OF CONTENTS

LIST OF ILLUSTRATIONS

LIST OF ILLUSTRATIONS (Contd)

LIST OF ILLUSTRATIONS (Contd)

LIST OF ILLUSTRATIONS (Contd)

LIST OF TABLES

GARRETT TURBINE ENGINE COMPANY
A DIVISION OF THE GARRETT CORPORATION
PHOENIX, ARIZONA

THERMAL BARRIER COATING LIFE-PREDICTION MODEL DEVELOPMENT SECOND ANNUAL REPORT

1.0 SUMMARY

Thermal barrier coatings (TBCs) for turbine airfoils in high-performance engines represent an advanced materials technology with both performance and durability benefits. The foremost TBC benefit is the reduction of heat transferred into air-cooled components. To achieve these benefits, however, the TBC system must be reliable. Mechanistic thermomechanical and thermochemical life models and design data base are therefore required for the reliable exploitation of TBC benefits on gas turbine airfoils. Garrett's NASA-HOST Program is designed to fulfill these requirements.

This program focuses on predicting the lives of two types of strain-tolerant and oxidation-resistant TBC systems that are produced by commercial coating suppliers to the gas turbine industry. The plasma-sprayed TBC system, composed of a low-pressure plasma-spray (LPPS) or an argon shrouded plasma-spray (ASPS) applied oxidation resistant NiCrAlY (or CoNiCrAlY) bond coating and an air-plasma-sprayed yttria (8 percent) partially stabilized zirconia insulative layer (Figure 1-1), is applied by Chromalloy (Orangeburg, New York), Klock (Manchester, Connecticut), and Union Carbide (Indianapolis, Indiana). The second type of TBC is applied by the electron beam - physical vapor deposition (EB-PVD) process by Temescal (Berkeley, California).

The second year of this multiyear program was focused on the following activities:

- Specimen procurement
- TBC system characterization

GARRETT TURBINE ENGINE COMPANY
A DIVISION OF THE GARRETT CORPORATION
PHOENIX, ARIZONA

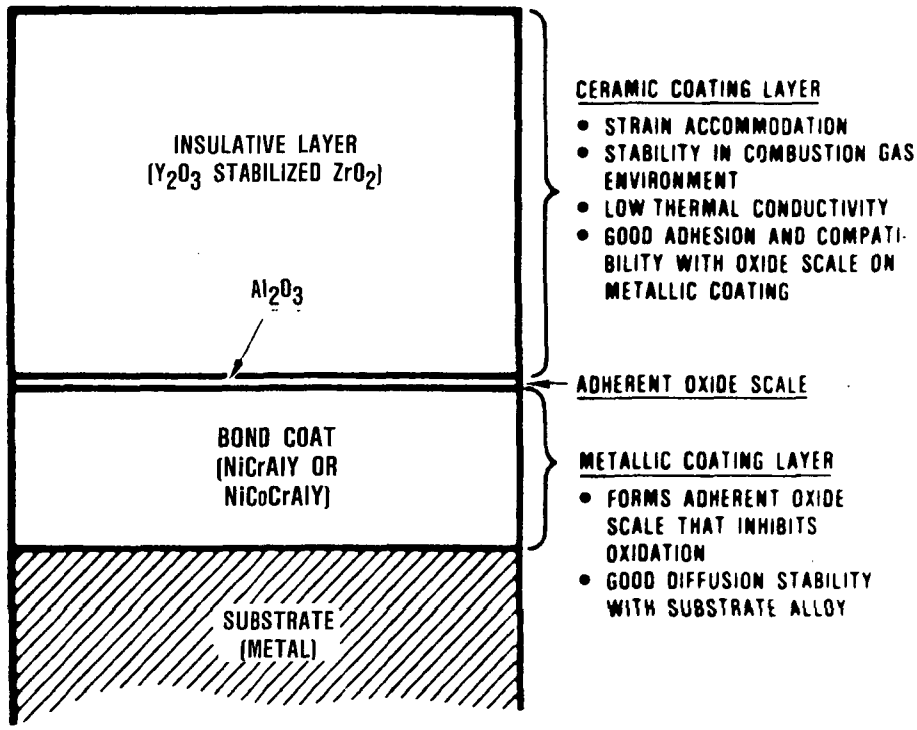

Figure 1-1. Constituents of a Thermal Barrier Coating System.

- o Nondestructive evaluation methods
- o Life prediction model development
- o TFE731 engine testing of thermal-barrier-coated (TBCed) HP turbine blades

The program consists of two phases. Phase I, Failure Mode Analyses and Model Development (Tasks I - V and A), is a 36-month technical effort and focuses on experimentally quantifying plasma-sprayed and EB-PVD failure modes and on developing engine-mission-analysis-capable preliminary TBC life prediction models for major failure modes. Task A is a GTEC-funded task providing for coating HP turbine blades with the specific coating systems selected for Phase I and conducting piggyback factory engine tests to provide data to verify the TBC life prediction model's accuracy.

Phase II, Design-Capable Life Models (Tasks VI-XI and B), is a 24-month optional effort to be exercised by NASA at the end of Phase I. It provides for additional experimental quantification of failure modes in plasma-sprayed TBCs and development of a comprehensive, mission-capable model with the desired accuracy for final designs. The mission-analysis capability of the TBC life model will be validated with analyses of multitemperature burner rig tests and factory test engine experience. In addition, GTEC-funded Task B provides for applying TBC systems that were successfully factory-tested in Task A to HP turbine blades. These blades will be made available for piggyback field engine tests. Available field test data will also be used to validate the TBC life models. Design capabilities of the TBC life analysis procedures will be applied to the design analysis of a high-performance thermal-barrier-coated (TBCed) HP turbine component.

Tasks I, II, IV, and A were active during this reporting period and encompass specimen procurement, data acquisition to calibrate and verify the materials life models, development of component life

models, NDE methods, and piggyback engine testing. These subjects are reviewed in the following sections.

2.0 INTRODUCTION

Thermal barrier coatings (TBCs) for turbine airfoils in high-performance engines represent an advanced materials technology that has both performance and durability benefits. Foremost of the TBC benefits is the reduction of heat transferred into air-cooled components. To achieve these benefits, however, the TBC system must be reliable. Mechanistic thermomechanical and thermochemical life models and a design data base are therefore required for the reliable exploitation of TBC benefits on gas turbine airfoils. This 60-month program is designed to fulfill these requirements.

GTEC strategy for this program comprises the following objectives:

- Development of mission-analysis-capable thermochemical and thermomechanical TBC life models that recognize and account for all significant mission, engine, and component design factors. These parameters include temperature, time, six TBC strain components, turbine pressure, and aircraft altitude (salt ingestion).

- Development of rapid computation approaches for estimating TBC life during preliminary design iterations.

- Development of a comprehensive TBC life model to provide the desired accuracy for final component designs.

- Obtaining design data for plasma-sprayed and electron beam evaporation - physical vapor deposition (EB-PVD) TBC systems produced by commercial suppliers to the gas turbine industry; i.e., Chromalloy, Klock, Union Carbide, and Temescal.

Materials testing in this program is approaching completion. Thermomechanical characterization of the TBC systems, with toughness, and spalling strain tests, has been completed. Modulus testing is in progress. Thermochemical (burner rig) testing is approximately two-thirds complete.

Three failure modes - bond coating oxidation, zirconia sintering (toughness reduction), and molten salt film damage, have been observed to govern TBC life. Preliminary materials life models for the first two of these failure modes have been developed. Integration of these life models with airfoil component analysis methods is also in progress with the goal of predicting TBC life in terms of engine, mission and materials system parameters.

Eddy current technology feasibility has been established with respect to nondestructively measuring zirconia layer thickness of a TBC system.

Testing of high pressure turbine blades coated with the program TBC systems is in progress in a TFE731 turbofan engine. Data from this test will be used to validate the TBC life models.

3.0 TBC SYSTEMS AND SPECIMEN PROCUREMENT

The objective of this program is to develop life prediction methods for plasma-sprayed and EB-PVD TBC systems. This effort is focused on the following TBC systems applied by four commercial suppliers:

Chromalloy - NiCrAlY (LPPS) + 8 percent Y_2O_3 stabilized ZrO_2 (APS)

Klock - NiCrAlY (LPPS) + 8 percent Y_2O_3 stabilized ZrO_2 (APS)

Union Carbide - CoNiCrAlY (ASPS) + 8 percent Y_2O_3 stabilized ZrO_2 (APS)

Temescal - NiCoCrAlY (EB-PVD) + 20 percent Y_2O_3 stabilized ZrO_2 (EB-PVD)

Compositions and microstructures of these TBC systems are reviewed in the following paragraphs.

Low pressure plasma-spray (LPPS) and argon shrouded plasma-spray (ASPS) processes were used to apply oxidation-resistant bond coating. The insulative 8 percent Y_2O_3 - ZrO_2 layers were applied by air plasma-spray (APS). Specimens were coated using the fixed (proprietary) processes of Chromalloy Research and Technology in Orangeburg, New York, Klock in Manchester, Connecticut, and Union Carbide, in Indianapolis, Indiana. Microstructures of the Chromalloy, Klock and Union Carbide plasma-sprayed TBC systems are provided in Figures 3-1, 3-2, and 3-3, respectively.

EB-PVD coatings were applied by Temescal in Berkeley, California using their established (proprietary) fixed process. The EB-PVD TBC system featured a columnar grained EB-PVD applied yttria

GARRETT TURBINE ENGINE COMPANY
A DIVISION OF THE GARRETT CORPORATION
PHOENIX, ARIZONA

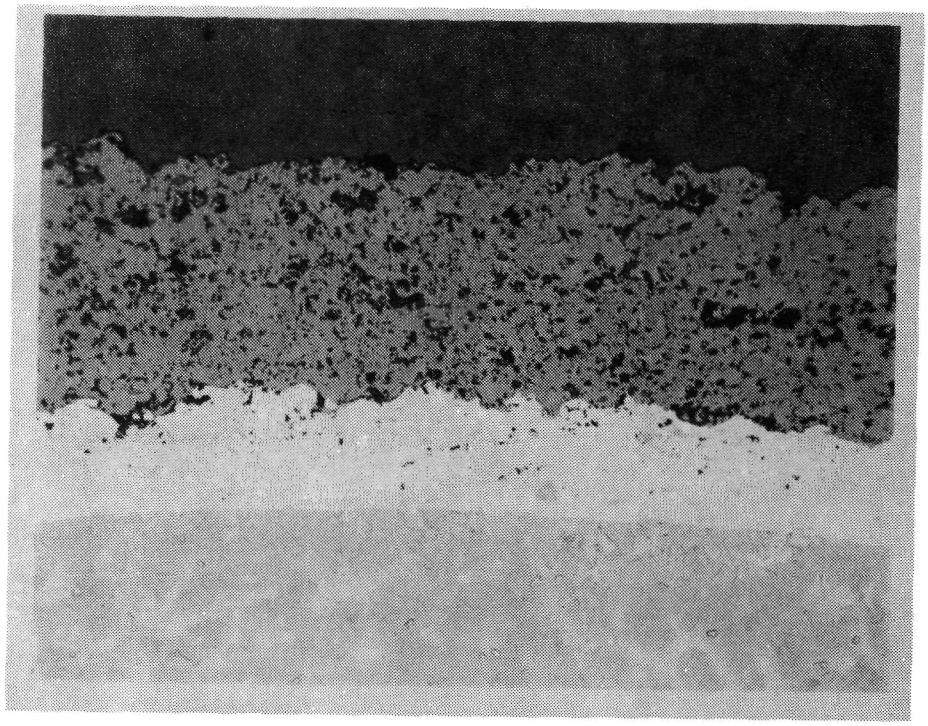

Figure 3-1. Pretest Microstructure of Chromalloy Plasma-Sprayed Ni-31Cr-11Al-0.5Y Plus Y_2O_3 (8 Percent) Stabilized ZrO_2 Thermal Barrier Coating System, 200X Magnification.

GARRETT TURBINE ENGINE COMPANY
A DIVISION OF THE GARRETT CORPORATION
PHOENIX, ARIZONA

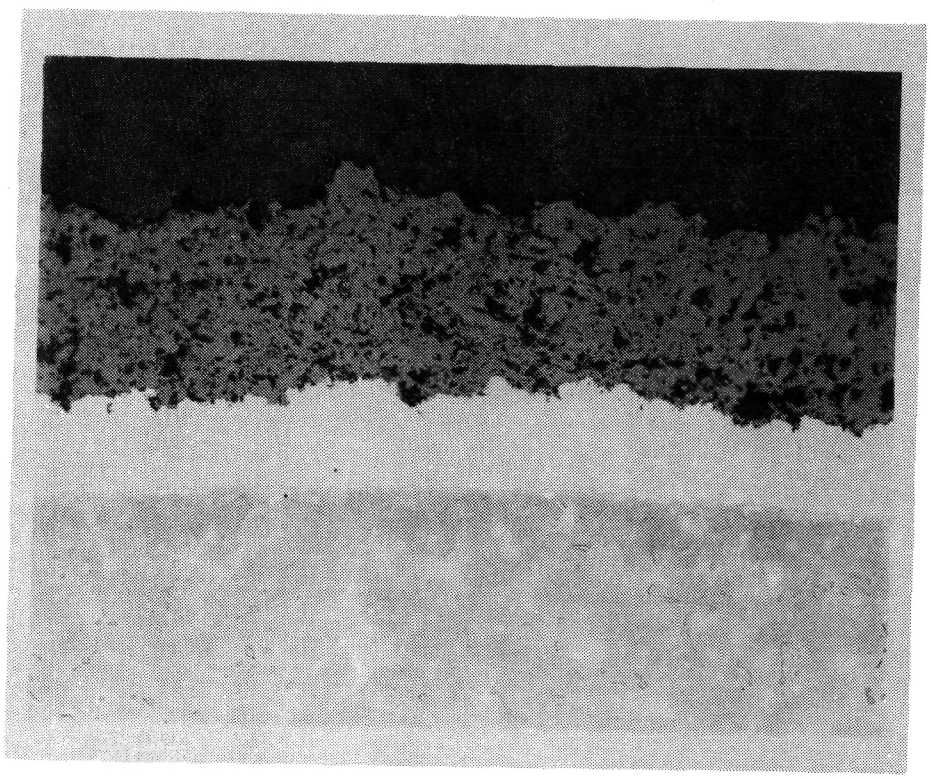

Figure 3-2. Pretest Microstructure of Klock Plasma-Sprayed Ni-31Cr-11Al-0.5Y Plus Y_2O_3 (8 Percent) Stabilized ZrO_2 Thermal Barrier Coating System, 200X Magnification.

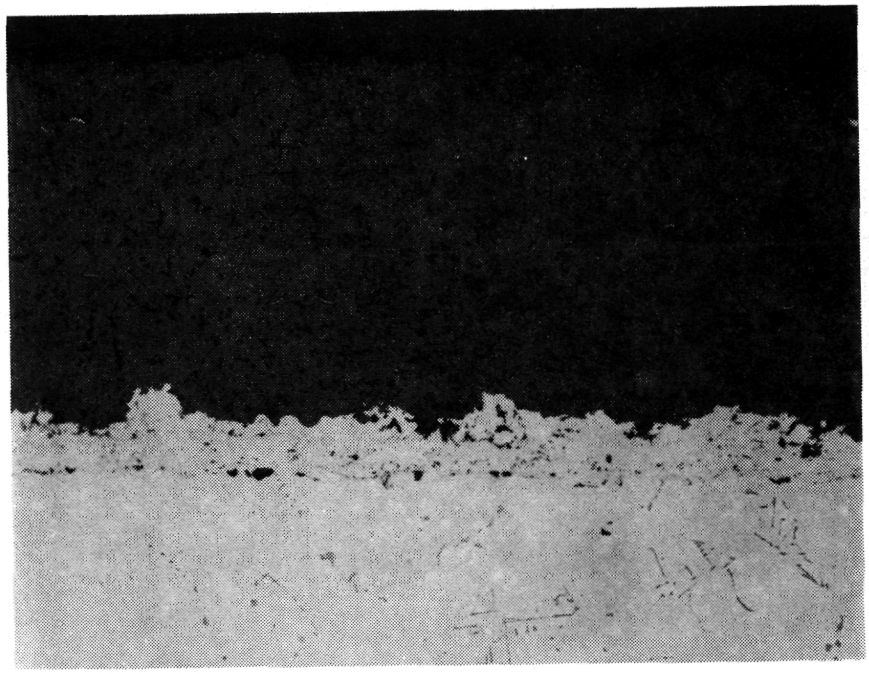

Figure 3-3. Pretest Microstructure of Union Carbide Plasma-Sprayed 39Co-32Ni-21Cr-8Al-0.5Y Plus Y_2O_3 (8 Percent) Stabilized ZrO_2 Thermal Barrier Coating System, 200X Magnification.

(20 percent) fully stabilized cubic zirconia insulative layer on top of a Ni-23Co-18Cr-11Al-0.3Y EB-PVD oxidation resistant bond coating. The microstructure of the EB-PVD TBC system is provided in Figure 3-4.

Capabilities of these TBC systems are being established on several types of specimens machined from Mar-M247 superalloy castings. The composition of this alloy is provided in Table 3-1. The cast Mar-M 247, which is used in the equiaxed and directionally solidified conditions for turbine airfoils, was selected for all specimens because of its stability at elevated temperature for long exposure times. Burner rig test specimen, cohesive/interfacial strength and toughness specimens, thermal conductivity samples, tension and compression spalling strain samples, and the modulus specimen are shown in Figures 3-5 through 3-9. The cohesive strength specimen was also used for evaluating nondestructive evaluation (NDE) feasibility.

TABLE 3-1. COMPOSITION OF MAR-M247 SUPERALLOY (WEIGHT PERCENT)

	Mo	W	Ta	Al	Ti	Cr	Co	Hf	Zr	C	B	Ni
MAR-M 247	0.65	10.0	3.3	5.5	1.05	8.4	10.0	1.4	0.055	0.15	0.015	Balance

The solid Mar-M 247 spalling strain specimens were used to replace IN718 tube specimens [1]*, which were prone to wall thickness variations, buckling concurrent with zirconia spalling in compression, and metallurgical instability during post-coating exposures at high temperatures.

*References are listed at the back of the text.

GARRETT TURBINE ENGINE COMPANY
A DIVISION OF THE GARRETT CORPORATION
PHOENIX, ARIZONA

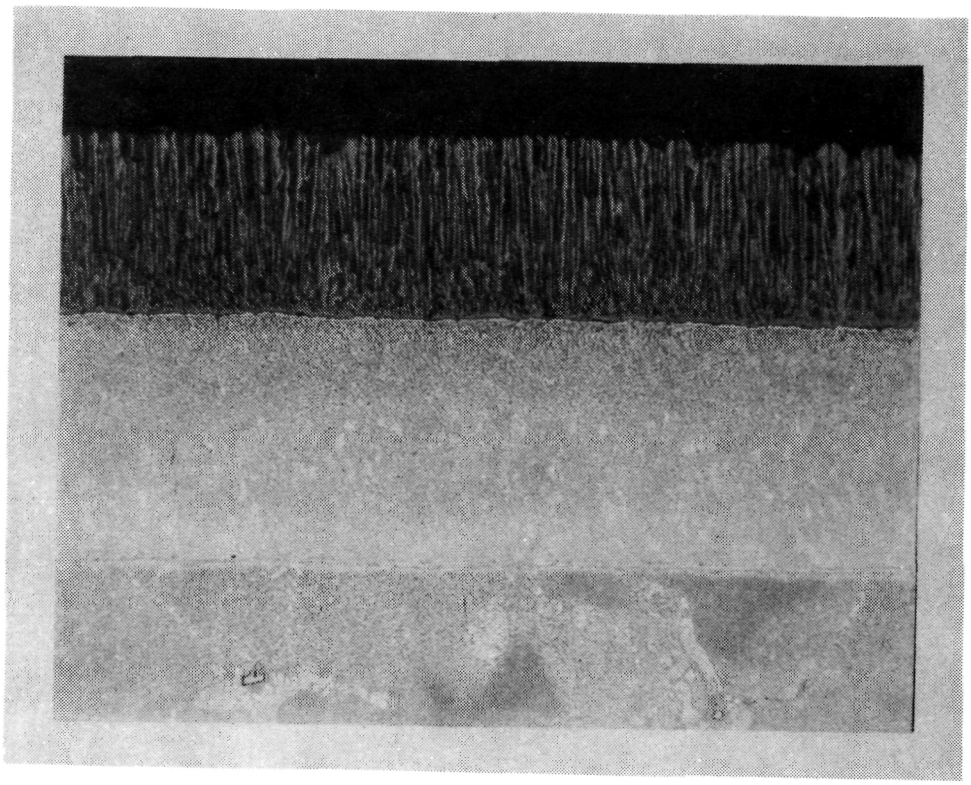

Figure 3-4. Pretest Microstructure of Temescal EB-PVD Ni-23Co-18Cr-11Al-0.3Y Plus Y_2O_3 (20 Percent) Stabilized ZrO_2 Thermal Barrier Coating System, 200X Magnification.

GARRETT TURBINE ENGINE COMPANY
A DIVISION OF THE GARRETT CORPORATION
PHOENIX, ARIZONA

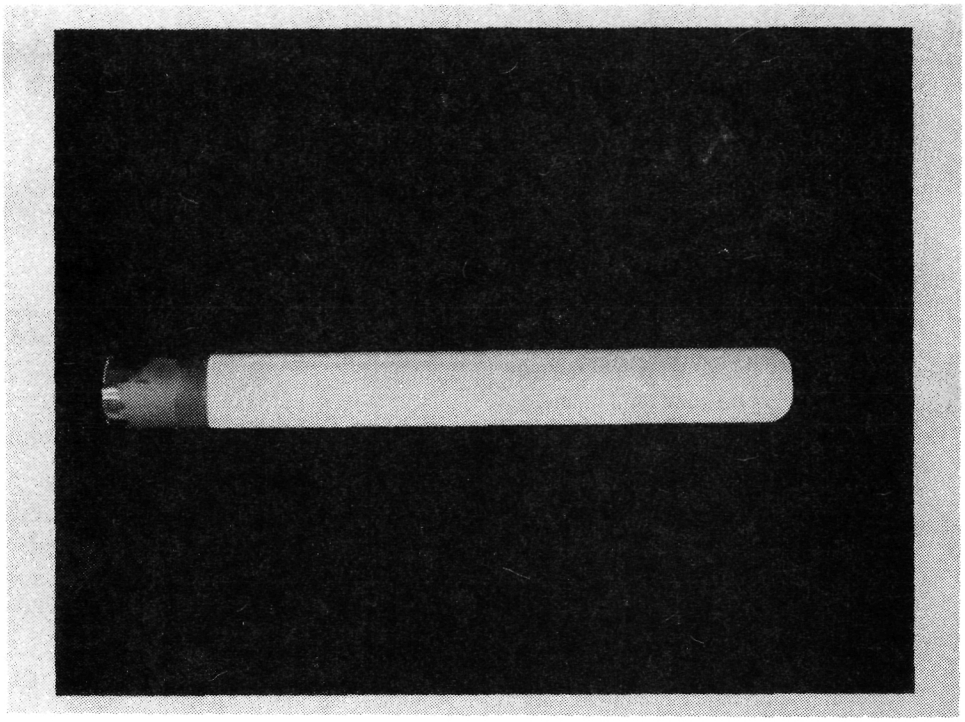

Figure 3-5. Burner Rig Specimens are Used to Calibrate Environmental Life Model.

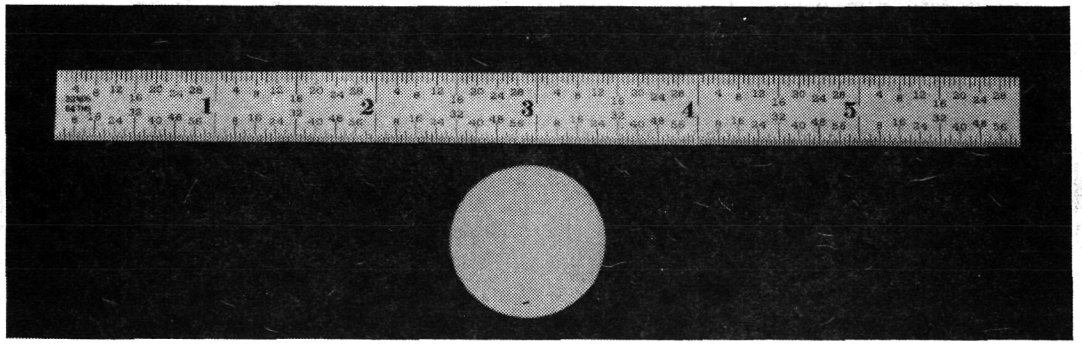

Figure 3-6. Cohesive (Interfacial) Strength and Toughness Specimen is used to Obtain Fracture Mechanics Data. This Specimen is also Used for NDE Feasibility Studies.

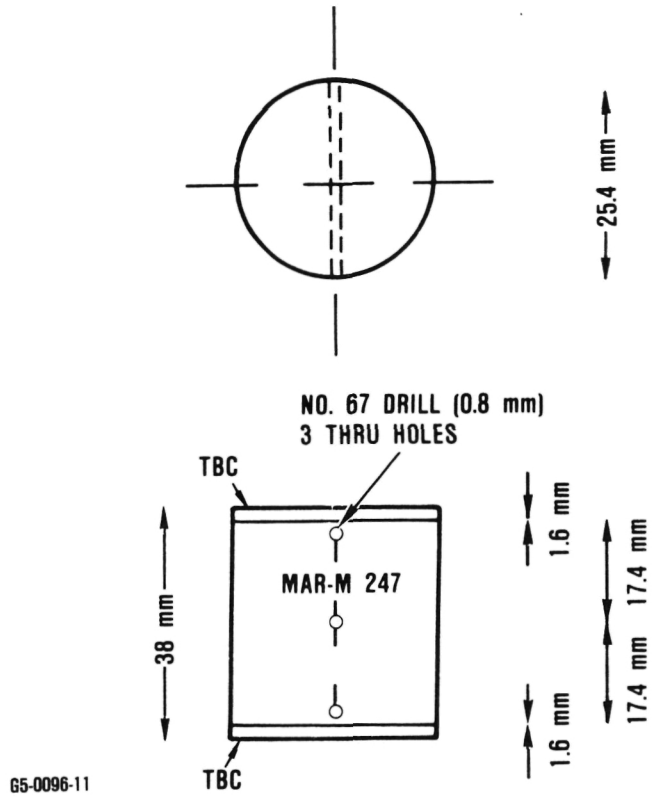

Figure 3-7. Thermal Conductivity Specimens are used to Quantify Heat Conductance of Thermal Barrier Coating System.

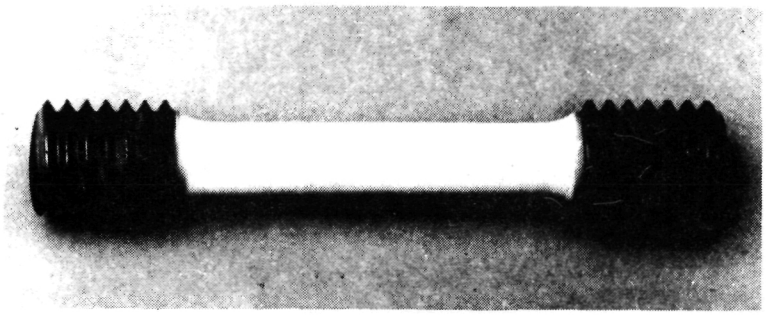

TENSION

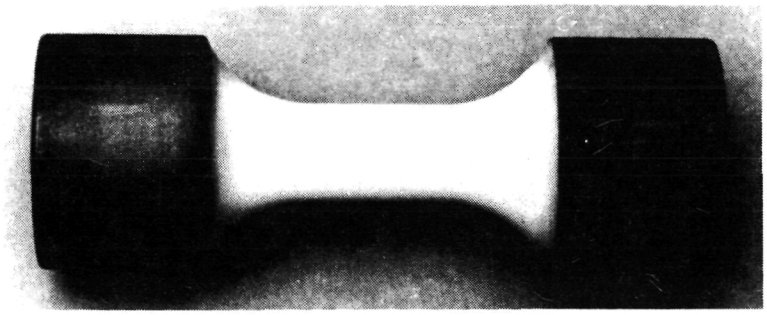

COMPRESSION

Figure 3-8. Solid MAR-M 247 TBC Coated Samples were used to Obtain the Spalling Strain Data for the Chromalloy and Temescal TBC Systems.

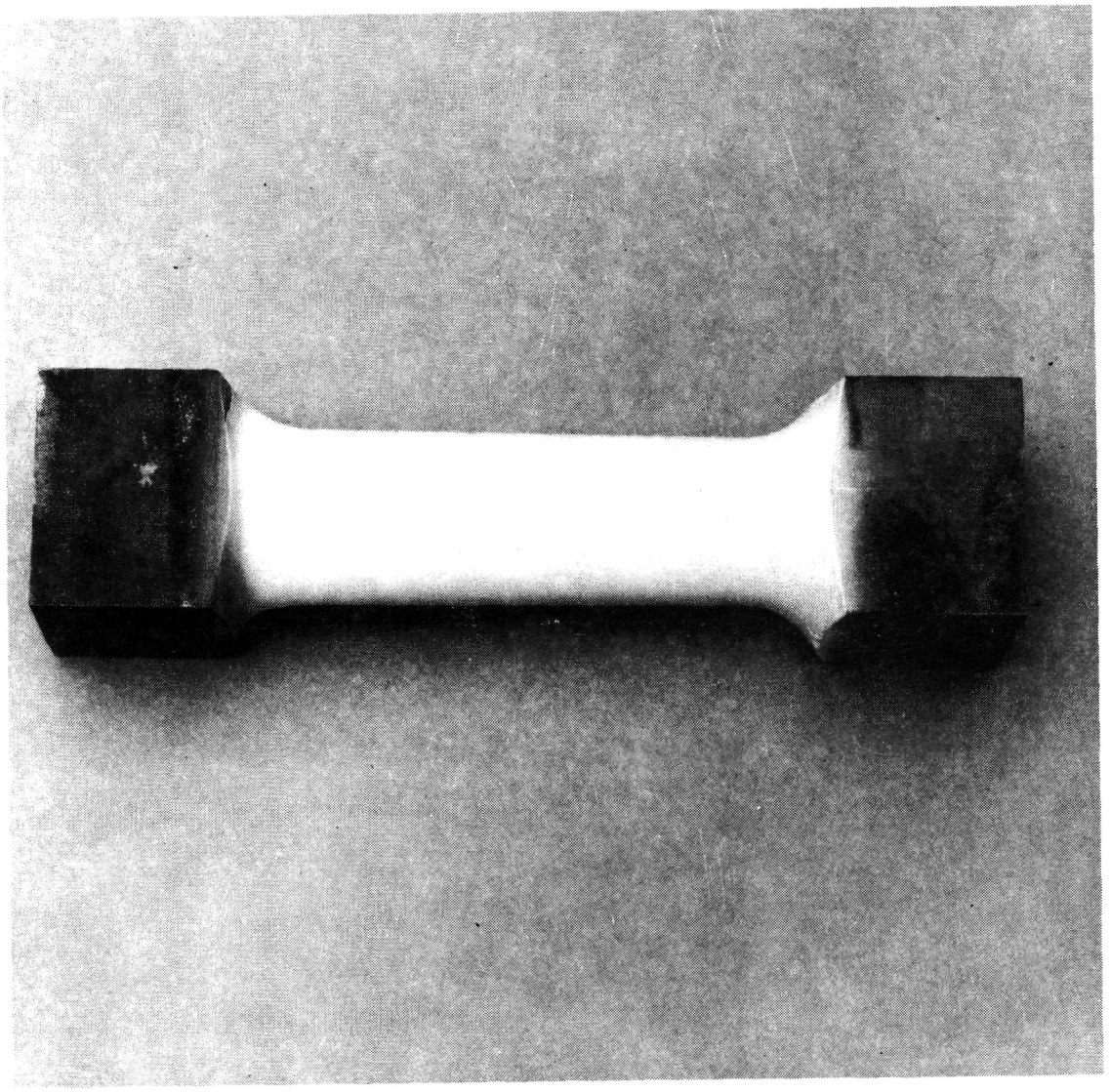

Figure 3-9. Modulus Data for the ZrO_2 and Bond Coat were Determined with a Thin Wall Sample Made of MAR-M 247.

4.0 TBC SYSTEM CHARACTERIZATION

In preparation for the development of thermomechanical and thermochemical models for TBC life, the TBC systems are being characterized for strength and toughness, tensile and compressive spalling strains, oxidation and molten salt film damage, and thermal conductivity. In addition, feasibility is being assessed for NDE methods to quantify TBC thickness, flaw sizes and insulative capability. The status of these investigations is reviewed in the following paragraphs.

4.1 TBC Strength and Fracture Toughness

Biaxial compressive stresses within the plane of the zirconia coating result in tensile stresses within the zirconia perpendicular to the plane of the ceramic-metal interface. Zirconia layer spalling can occur when these stresses exceed critical values, which are flaw size dependent.

In order to predict the viability of a TBC system, it is necessary to quantify the strength and toughness (flaw size dependence of strength) of the zirconia layer (plasma sprayed TBCs) or the zirconia-bond coating interface (EB-PVD TBCs). Therefore, a series of bond strength tests, with and without artificial flaws at or near the interface were conducted to obtain the required data. Toughnesses of the zirconia or zirconia-bond coating interface were determined in both the as-received condition and after thermal exposures at high temperatures (1100 and 1150C) characteristic of turbine engine applications.

Cohesive strength data for the plasma-sprayed zirconia were obtained by epoxy bonding TBCed bond specimens (Figure 4-1) into threaded pull rods and loading to fracture in a universal tensile test machine. Fracture toughness of the zirconia was obtained by

GARRETT TURBINE ENGINE COMPANY
A DIVISION OF THE GARRETT CORPORATION
PHOENIX, ARIZONA

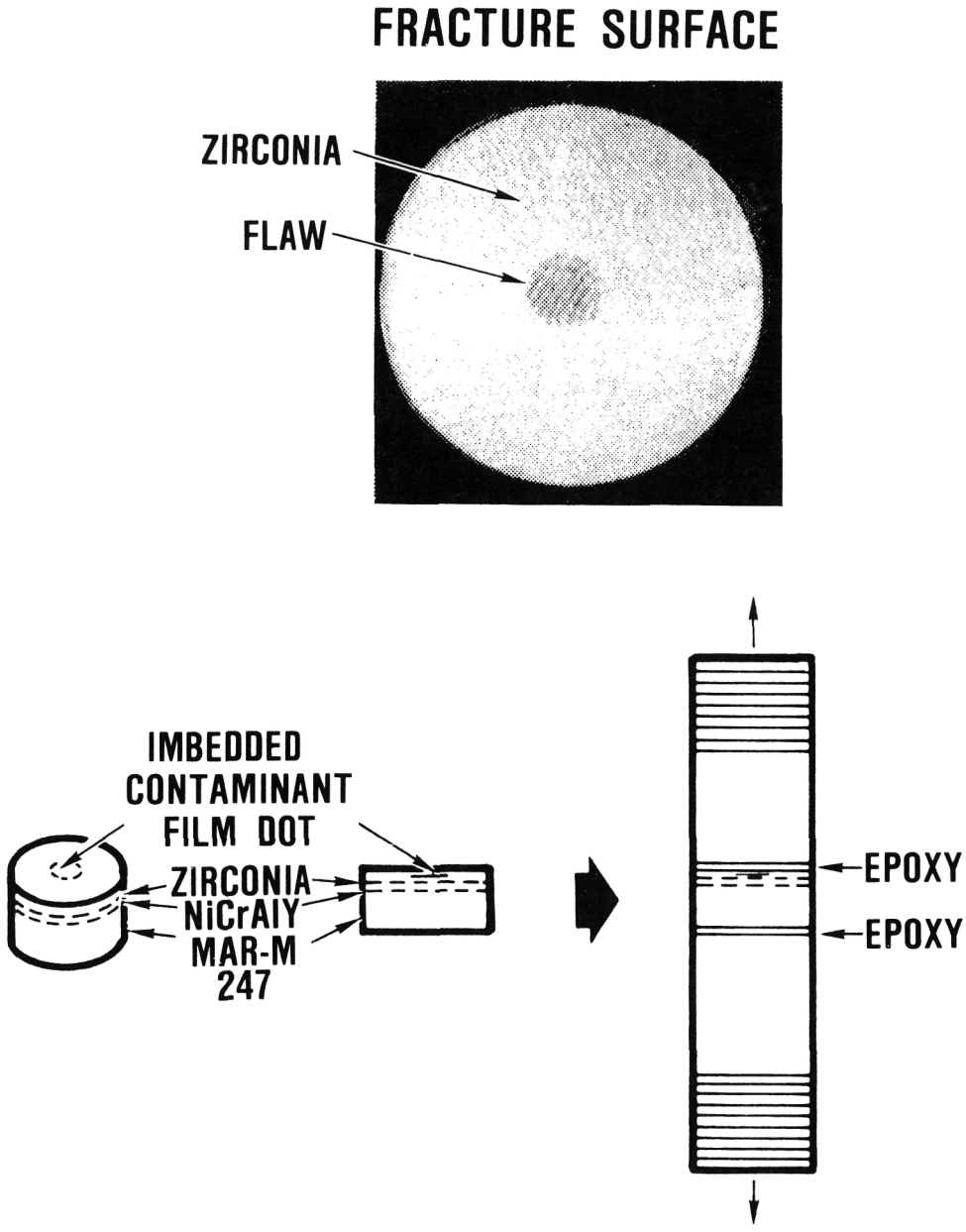

Figure 4-1. Cohesive and Interfacial Toughness of TBC System can be Quantified with Modified Bond Strength Test.

briefly interrupting coating and incorporating an artificial (vacuum grease) flaw of known diameter into the zirconia coating layer and testing in a similar manner. The fracture toughness relationship for a penny-shaped crack in an infinite body subjected to uniform tension,

$$K_{Ic} = 2/\sqrt{\pi}\ \sigma_f \sqrt{c/2} \qquad (1)$$

where σ_f is the fracture strength of the flawed specimen and c is the flaw diameter, was used to estimate the fracture toughness of the yttria partially stabilized zirconia layer.

Cohesive toughness data were obtained with the Chromalloy and Union Carbide specimens in several "pre-test" conditions, which included short post-coating heat-treatments, and after longer exposures at 1100 and 1150C. Post-test visual examination confirmed that the artificial flaw within the zirconia layer initiated the preliminary crack. As indicated in Figure 4-2, crack propagation typically remained within the zirconia layer for all of the Chromalloy specimens and for Union Carbide specimens with shorter exposures at 1100 and 1150C. For Union Carbide specimens exposed for longer times (300 hours at 1100C and 30 hours at 1150C), the cracks propagated only a short distance within the zirconia before the crack path changed to the oxidized interface. The change in crack path is illustrated in Figure 4-3. This result is thought to imply that the toughness of the oxidized interface has become lower than the zirconia layer. In contrast, flaw propagation remained within the Chromalloy zirconia layer for the range of thermal exposures investigated.

An engine mission analysis capable fracture mechanics approach to predicting zirconia spalling stresses requires that the zirconia

GARRETT TURBINE ENGINE COMPANY
A DIVISION OF THE GARRETT CORPORATION
PHOENIX, ARIZONA

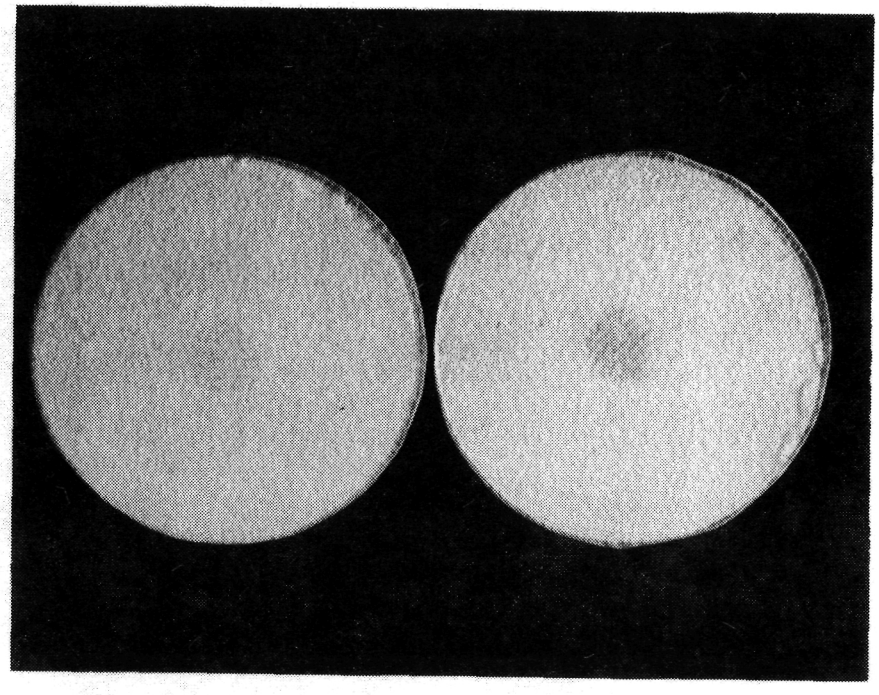

Figure 4-2. An Artificial 6-mm-Diameter Flaw Initiated Fracture in the Zirconia Layer of a Chromalloy Coated Cohesive Toughness Specimen.

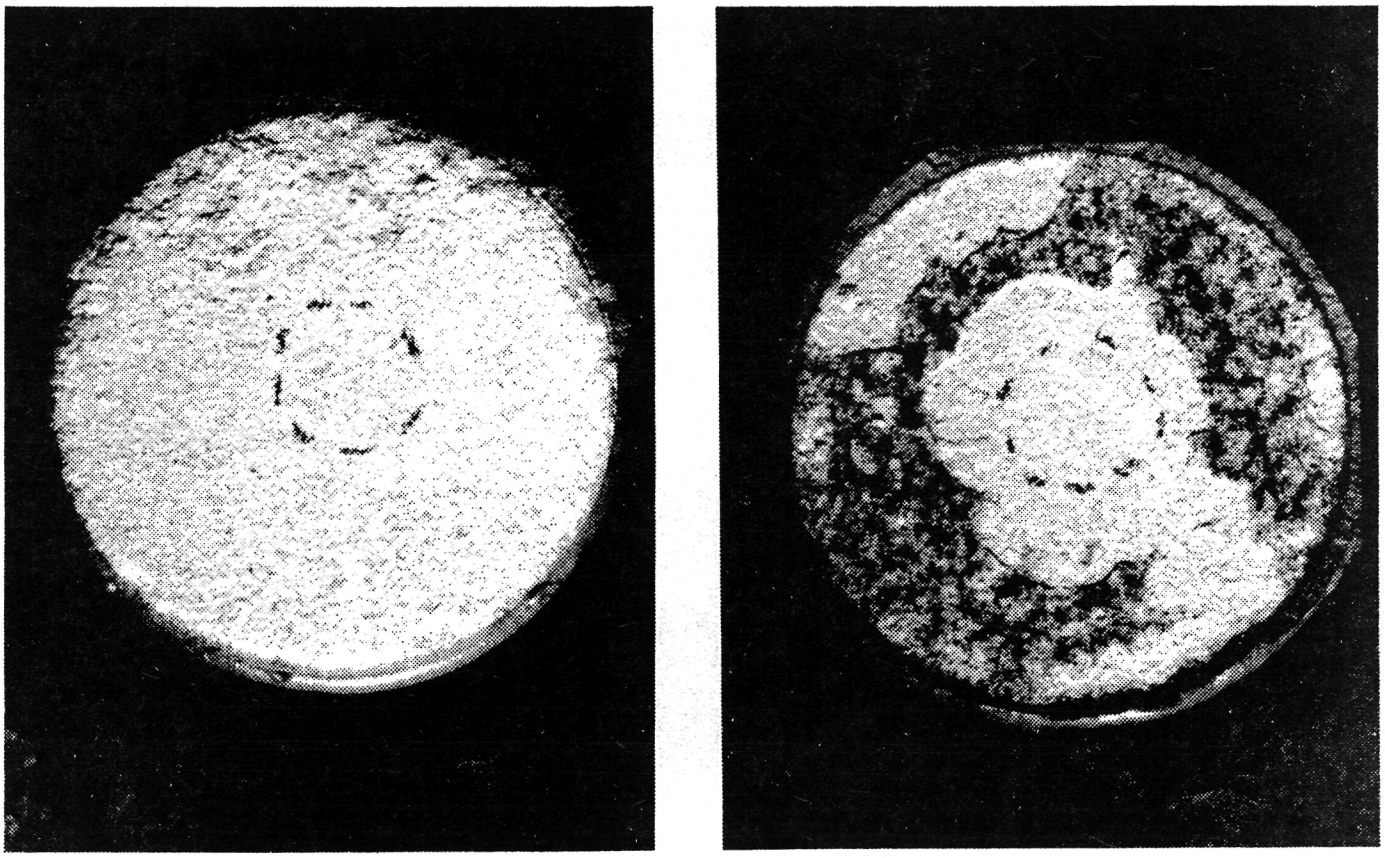

3 Hours at 1100C
K_{IC} = 1.05 MPa $\sqrt{m}$
Specimen: U15K6-18

300 Hours at 1100C
K_{IC} = 0.62 MPa $\sqrt{m}$
Specimen: U15K6-10

Figure 4-3. Longer Exposure Times Favored Crack Propagation Along the Oxidized CoNiCrAlY/Zirconia Interface.

toughness be quantified as a function of high temperature exposure time and temperature. It is also desirable that acceptable variations in zirconia processing, composition and microstructure be included in the toughness data base. Therefore, zirconia fracture toughness data for both Union Carbide and Chromalloy TBC systems are shown as a step function of exposure time at 1100C and 1150C in Figures 4-4 and 4-5 respectively. Although other functional relationships may be possible to represent these data, the step function is preferred since it facilitates component analysis as a function of exposure time and temperature. Combining the data for Chromalloy and Union Carbide TBC systems also permits effects of production source variations to be assessed from a data scatter standpoint.

Pretest and shorter time exposure data (both 1100 and 1150C), which had relatively high values of toughness, were used to establish the typical and typical minus 2 standard deviations values for the upper shelf. Longer exposure time, lower toughness data were similarly analyzed to estimate the typical and typical minus 2 standard deviations values for the lower shelf. Transition from the upper to lower shelf values of toughness were analyzed as an assumed linear relationship between temperature and the logarithm of transition time. Transition times are currently shown as vertical lines. However, a more gradual transition between the upper and lower shelf values of toughness may be more realistic. The analytical expression for toughness that will be utilized for preliminary design modeling is as follows:

$$K_{Ic} = 0.91 + 0.235 \tanh (\exp [-0.041(T+273)+61.15] - t) \text{ MPa } \sqrt{m} \qquad (2)$$

where T is the temperature in C and t is the time in hours.

No significant differences were observed between the toughness data for the Chromalloy and Union Carbide zirconia after exposures

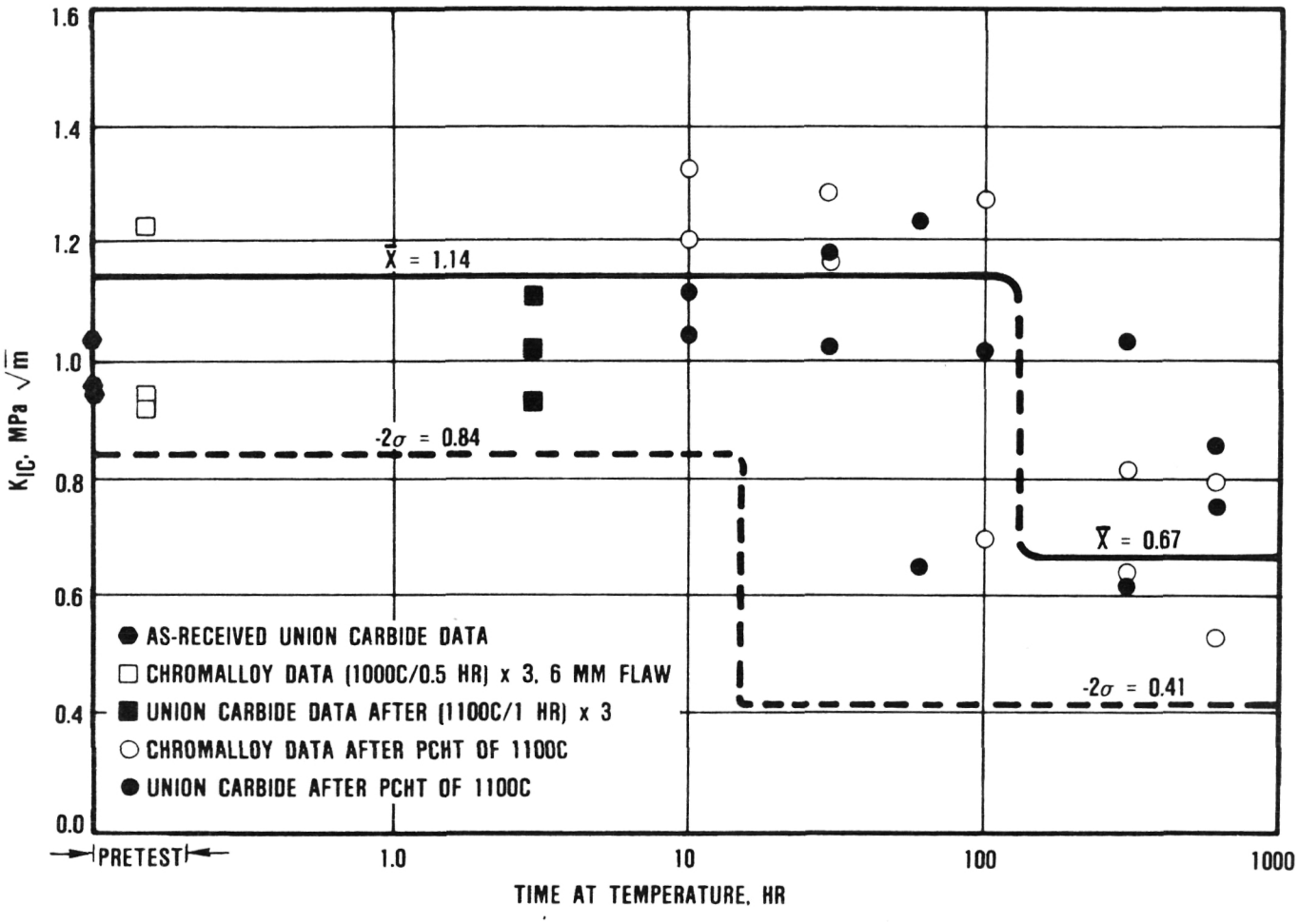

Figure 4-4. Fracture Toughness of Plasma Sprayed Yttria (8 Percent) Stabilized Zirconia is Reduced After Long Exposures at 1100C.

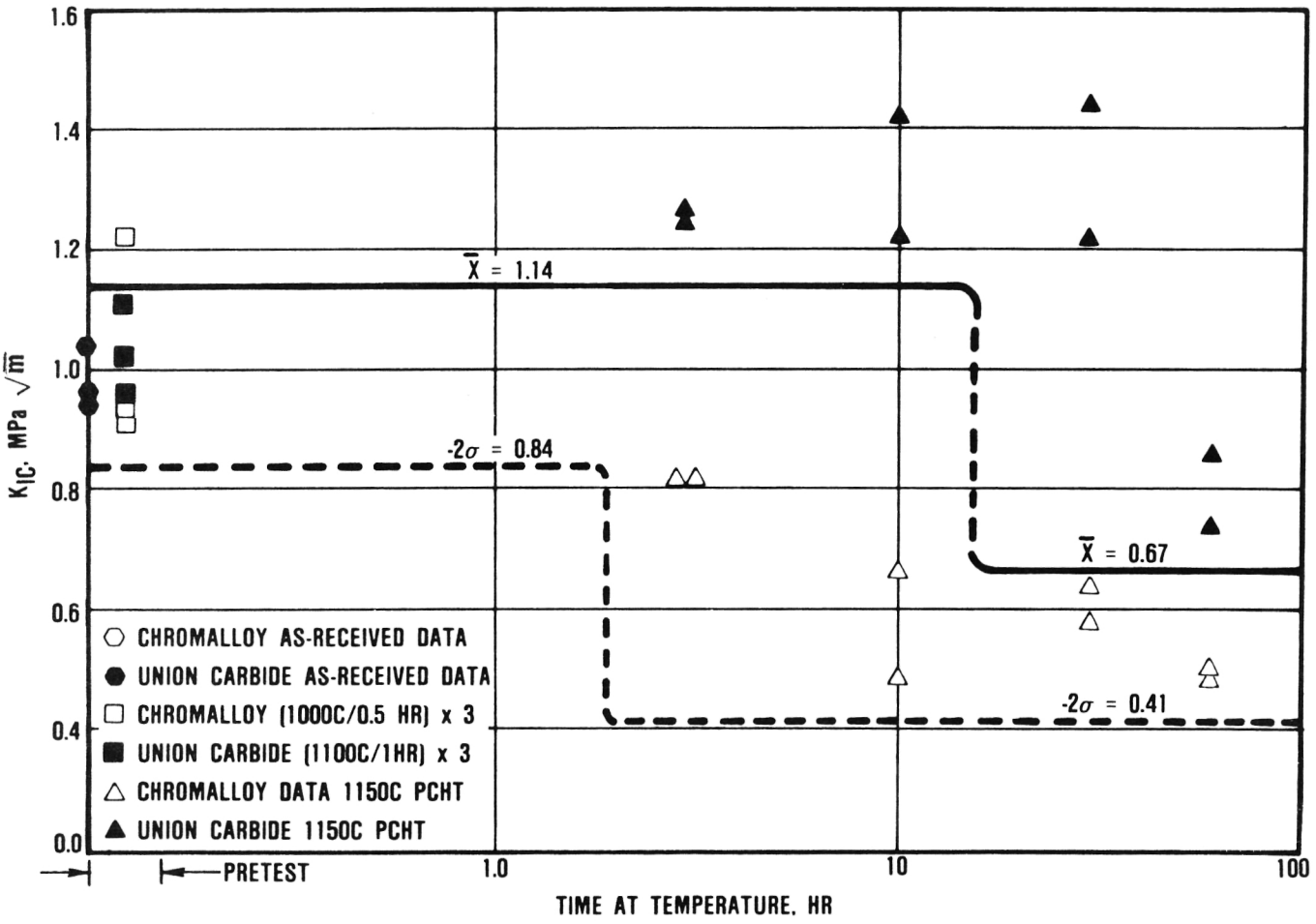

Figure 4-5. Fracture Toughness of Plasma Sprayed Yttria (8 Percent) Stabilized Zirconia is reduced After the Longer Exposures at 1150C.

at 1100C. On the other hand, the Union Carbide coatings had higher toughness after exposure at 1150C than the Chromalloy TBCs. (If the flaw was placed at the oxidized interface, however, the ranking would be expected to reverse.)

Cohesive strength tests were also performed on the Chromalloy and Union Carbide TBC systems using specimens without artificial flaws in order to obtain an estimate of the inherent flaw size present within the TBC system. In most instances failure occurred within the epoxy rather than the zirconia when artificial flaws were absent. In several instances, however, cracking did initiate within the zirconia layer adjacent to the bond coating interface, as indicated in Figure 4-6. Re-arranging the fracture mechanics relationship (equation 1) permitted an effective circular flaw size to be calculated, which was under 2.8 mm in diameter in all cases. (In reality, actual flaws present within the zirconia layer are probably a few closely spaced microcracks that can easily link-up rather than a single circular flaw.)

Cohesive strength and toughness tests conducted with the Klock TBC system were inconclusive because the epoxy wicked completely through the zirconia to the NiCrAlY/zirconia interface. The epoxy wicking problem was attributed to a greater amount of interconnected porosity in the Klock specimens. In an effort to eliminate epoxy wicking through the Klock zirconia, several specimens were sprayed with an additional 250 μm of zirconia prior to bonding. A small amount of cobalt aluminate (about 0.1 percent) was added to the additional zirconia layer to provide a sufficient color difference to distinguish between the Klock zirconia and the added layer. Unfortunately, visual examination of the specimens indicated that the vacuum grease flaws within the Klock specimens did not initiate the crack which led to specimen failure. Instead, the primary crack seemed to initiate at the edge of the specimen in the doped zirconia coating or at the interface between the doped zirconia/Klock

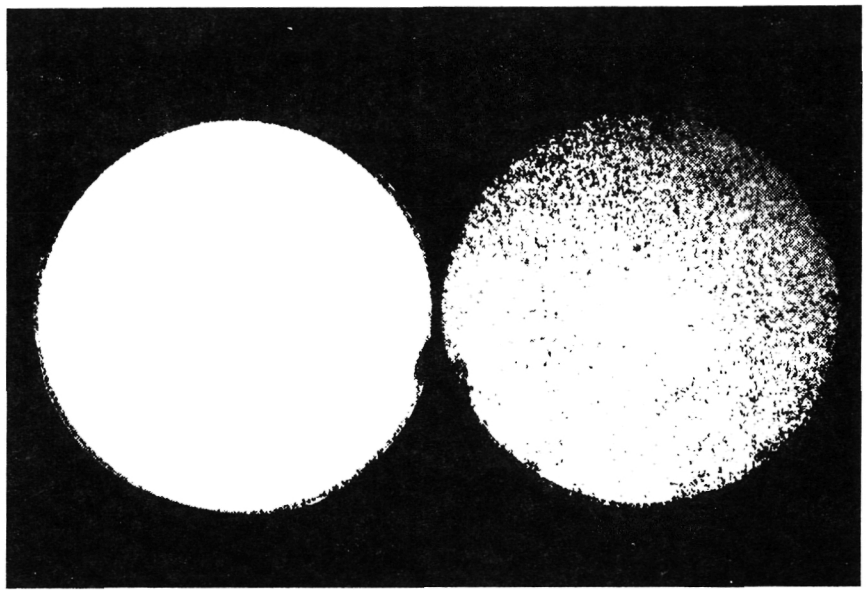

Figure 4-6. Cohesive Strength Failures of Chromalloy TBC System Occur Adjacent to the NiCrAlY/Zirconia Interface.

zirconia layer. None of the unflawed specimens failed within the Klock zirconia layer.

Failure of the Temescal EB-PVD TBC system typically initiates within the interfacial zone between the NiCoCrAlY bond coating and columnar zirconia layers. This one to four micron-thick zone consists of the oxidation resistant alumina scale and a relatively dense, non-columnar zirconia layer, which is less than 2 microns-thick when the coating is properly processed.

In order to characterize the toughness of the EB-PVD TBC system, 1 and 3 mm diameter carbon dots were sputtered onto the NiCoCrAlY layer, which formed an artificial flaw, prior to deposition of the zirconia layer. Specimens were then tested in the as-received and thermally exposed conditions in an equivalent manner to that of the plasma sprayed TBC systems.

Unfortunately, the flaw sizes selected were, in most cases, insufficient to initiate interfacial failure before the epoxy failed.

Only two specimens failed at the NiCoCrAlY/zirconia interface. Calculated interfacial toughnesses were 1.9 and 1.6 MPa $\sqrt{m}$ after 1 and 30 hour exposures at 1150C. All other tested specimens failed at locations other then the interface, which is consistent with high toughness. In a GTEC R&D study in which 4 mm diameter flaws were used, about 75 percent of the specimens produced useful toughness data. Values were similar to those obtained in this program. Six mm diameter flaws have been successfully used in an Air Force sponsored program (F33615-85-C-5155). As-received toughnesses for this system were slightly greater than 2 MPa $\sqrt{m}$ in this program.

Six of the specimens exposed at 1150C had the zirconia layer spall during the thermal exposure. The inner half of the zirconia

thickness was almost transparent and appeared to be of high density. Microstructural examination of a specimen indicated that the columnar grains were sintering together.

All six of these specimens had been coated concurrently. A review of process records at Temescal indicated that the oxygen flow rate had been only 30 to 50 percent of that normally used to maintain zirconia stoichiometry. It is thought that the slightly oxygen deficient zirconia absorbed oxygen and expanded during the 1150C exposure, which put the columnar zirconia grains into compressive contact, facilitating sintering and subsequent spalling.

4.2 Zirconia Spalling Strain

In service, a TBC system will be exposed to both compressive and tensile strains at different points of a mission cycle. Consequently, the strain capabilities of the plasma sprayed and EB- PVD TBCs were determined at room temperature and 1000C to establish the strain tolerance of each system.

Spalling strain tests were performed in both tension and compression using the solid Mar-M 247 specimens shown in Figure 3-8. Initiation of spalling was determined visually. Data from these tests are discussed in the following paragraphs.

Plasma sprayed TBCs applied by Chromalloy were tested in the as-received condition and after 10 hour exposures in air at 1100 and 1150C. The zirconia thickness for most of these tests was 125 μm, but in three instances the thickness was increased to 250 μm.

No significant differences in the spalling strains with respect to the post-coating heat treatment and thickness of the ZrO_2 layer were observed. However, the spalling strain increased substantially with test temperatures, as indicated by the 1000C data, as shown in

Figure 4-7. From a design standpoint, low temperature compression spalling strains were the most limiting. The mean value of the nineteen room temperature compression spalling strain data is 1.09 percent and the mean-3 sigma value is 0.5 percent compressive strain. Compression cracking was detected prior to actual spalling; mean and mean-3 sigma values for compression cracking strain were 0.91 percent and 0.48 percent, respectively. Therefore, the safe amount of compression in the Chromalloy TBC system is about 0.5 percent.

Results from the 1000C tension tests indicated that zirconia spalling occurred at a mean strain of 2.97 percent. Delamination of the NiCrAlY bond coating was observed in the tensile tests conducted at room temperature. Low values of zirconia spalling are associated with this unexpected occurrence. In previous tensile tests of tube specimens, zirconia spalling was not observed when the NiCrAlY remained bonded to the substrate.

Results from the IN 718 tube specimens [1] were in general agreement with the solid specimen data. The zirconia layer of the Chromalloy and Klock TBC systems did not spall when the specimens were pulled in tension. Numerous parallel tensile cracks were observed in the zirconia prior to specimen failure. This is shown in Figure 4-8. These cracks originated in the NiCrAlY bond coat and propagated into the zirconia layer (Figure 4-9). All of the compression specimens reached a strain of 0.85 or higher (1.5 percent average) prior to specimen buckling and zirconia spalling, which were typically concurrent.

Spalling strain testing was also conducted with Temescal's EB-PVD NiCoCrAlY/yttria stabilized zirconia TBC system. All of the EB-PVD TBCs had zirconia thicknesses of 125 microns. Unexpectedly, the average strain to spall the ZrO_2 layer in the room temperature compression tests was only 0.31 percent. The EB-PVD ZrO_2 did not

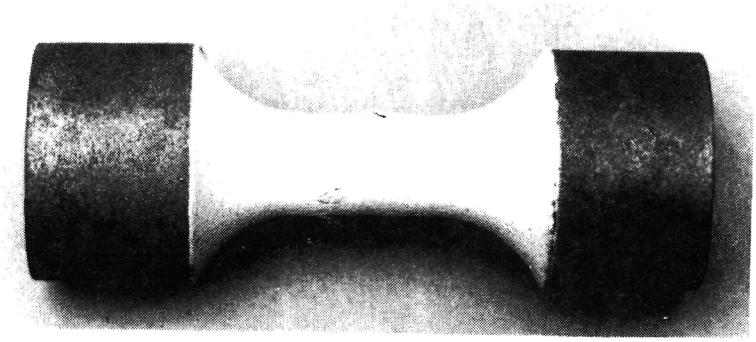

ROOM TEMPERATURE
COMPRESSIVE SPALLING STRAIN > 0.8 PERCENT

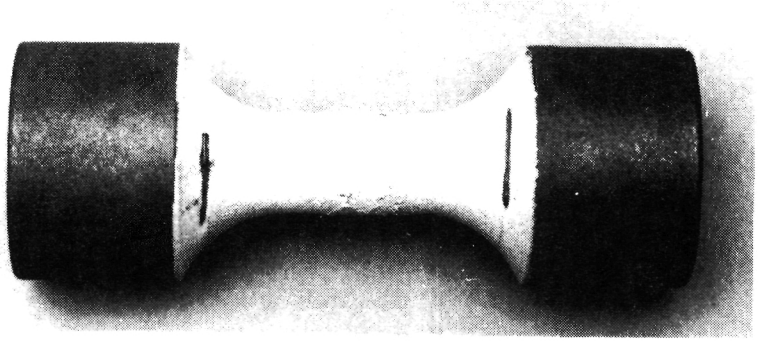

1000C
COMPRESSIVE SPALLING STRAIN >5 PERCENT

Figure 4-7. The Spalling Strain of Chromalloy's TBC System Increased with Test Temperature.

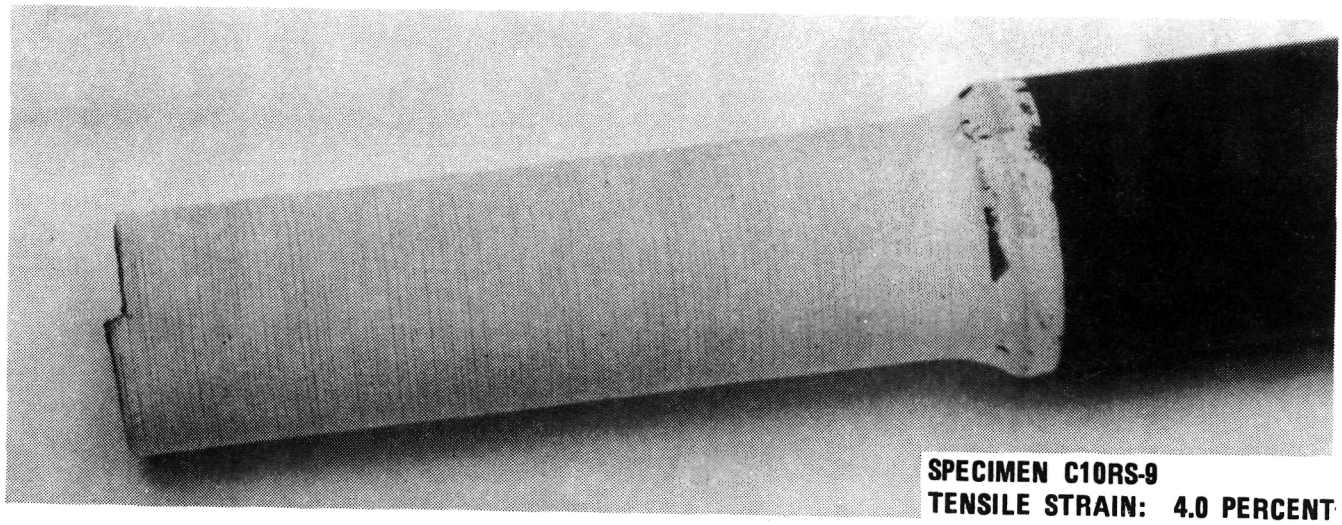

Figure 4-8. Zirconia Layer of Chromalloy TBC System did not Spall when the Specimen Failed. Numerous Parallel Tensile Cracks were Observed in the Zirconia.

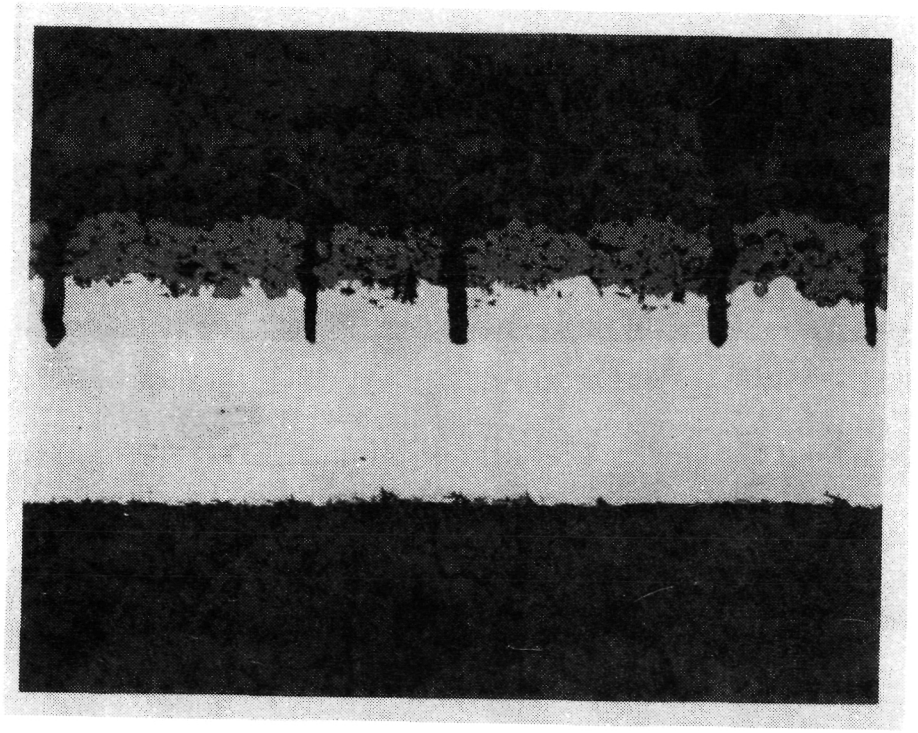

Figure 4-9. Tensile Cracks in the NiCrAlY and ZrO_2 Layers, 100X Magnification.

spall at 5 percent strain in the 1000C compression tests; however, the ZrO_2 subsequently spalled during cool down on 2 of 3 samples tested at 1000C. In tension, 1.95 percent was the mean value of the strain required to spall off the zirconia in both the room temperature and 1000C tests.

Based upon previous data for EB-PVD zirconia coatings reported by Sheffler [2], the low room temperature compression spalling strain were unexpected. Subsequent review of processing records at Temescal indicated that difficulties had been encountered during initial coating of the specimens and that the zirconia had been stripped and then recoated. It is speculated that this processing anomaly may have resulted in a marginally adherent alumina scale.

(It has been observed that initially formed alumina scales on NiCoCrAlY coatings are the most adherent. Also, initial oxide scale growth can result in yttrium depletion of the adjacent 50 microns of the NiCoCrAlY. If the initial oxide is stripped from the surface, there may be insufficient yttrium in the coating to promote the required adhesion of the subsequently formed alumina scale.)

After reviewing these data, Temescal stripped the compression specimens to the Mar-M 247 substrate and recoated the specimens. The process was slightly modified in that the NiCoCrAlY coating was lightly vapor honed after glass bead peening to remove any glass bead debris. Testing of these specimens indicated that the room temperature compression spalling strain increased to 1 percent, which is comparable with Sheffler's EB-PVD zirconia data [2] and the Chromalloy plasma sprayed zirconia data. A comparison of the zirconia spalling-strain data between Chromalloy's plasma-sprayed and Temescal's EB-PVD TBC systems is provided in Figure 4-10.

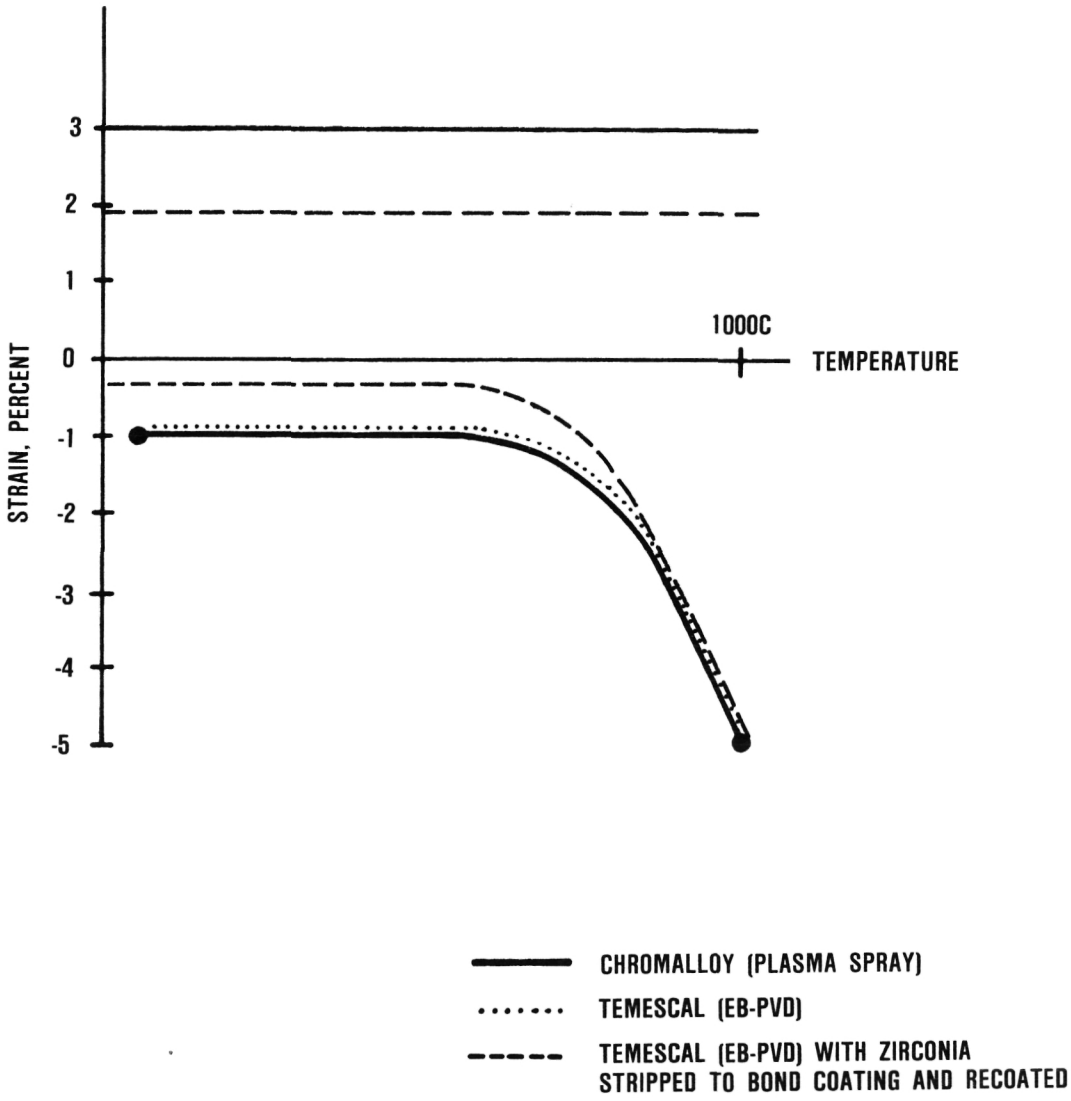

Figure 4-10. Compressive Strain at Low Temperatures is a Design-Limiting Factor.

4.3 Burner Rig Tests

A preliminary design model for predicting TBC life must be capable of rapid iteration in order to be a viable tool. Therefore, the Phase I preliminary design model is being tailored to be driven primarily by thermal analyses, engine cycle data and the planned flight spectrum for the aircraft. Stress analysis is intentionally limited, during these early design iterations, to verification that the TBC can survive a severe transient snap acceleration-deceleration cycle (i.e., idle to full power to idle with no intermediate power dwells).

Burner rig tests are the primary means for calibrating the preliminary design TBC materials models that quantify the thermally driven damage modes. Effects of bond coating oxidation and zirconia densification upon the time required to spall the zirconia layer are quantified with burner rig tests conducted in the 1020 to 1170C temperature range. Condensed molten sulfate salt films can be present upon the surface of a TBC when temperatures are below about 950C for aircraft operating in a predominately marine environment, such as maritime surveillance. Therefore, burner rig tests were conducted in the range of 780 to 935C to assess the significance of molten salt film damage with respect to zirconia layer spalling.

These tests were conducted in GTECs Mach 0.3 burner rig facility, which concurrently tests eight to twelve specimens in a carousel. . The test cycle was typically 27 minutes in the burner's exhaust followed by 3 minutes of forced air cooling. In one 1020C test, a shorter test cycle was employed (4 minutes hot plus 2 minutes forced air cooling) in order to assess cycle duration effects on TBC life. Coating thicknesses were typically 125 microns of bond coating and 125 microns of yttria stabilized zirconia for all systems. Specimens were examined visually twice daily for zirconia

spalling. A TBC was considered to be failed when 0.5 cm^2 of zirconia had spalled in the hot zone of the specimen.

Temperatures of the specimens were controlled by an optical pyrometer. Several times during a test (initially daily), the pyrometer was calibrated into agreement with two centerline thermocouples inserted into the hottest portion of two bars (middle of the heat tint pattern). Calibration of the optical pyrometer was always performed after steady-state metal temperatures and burner conditions were achieved. A subsequent survey indicated that, due to a hearth effect, a small gradient was present in the bars from the outside of the carousel to the inside, with the inside surface being about 20C hotter than the centerline thermocouple; similar results were reported by Sheffler and DeMasi, who are conducting comparable burner rig tests under contract NAS3-23944 [3].

Burner rig data for the plasma sprayed and EB-PVD systems are summarized graphically in Figures 4-11 and 4-12, respectively, for tests conducted with the 27 minutes hot plus 3 minutes forced air cool cycle. The scatter observed in Figure 4-11 is indicative of what might be anticipated for multiple production sources for a current generation plasma sprayed TBC. Similar scatter might be expected in Figure 4-12 if current generation EB-PVD TBC systems from different suppliers were tested.

Three damage mode regimens are indicated in these graphs. In the lowest temperature (780 to 945C) tests, the presence of salt deposits reduced the spalling life of the TBC systems. Oxidation of the bond coating was associated with TBC spalling at temperatures above 1000C. At still higher temperatures, zirconia densification (sintering) further accelerated TBC degradation.

Data were also obtained for a rapid (4 minutes hot plus 2 minutes forced air cool) burner rig cycle at 1020C to assess the effect

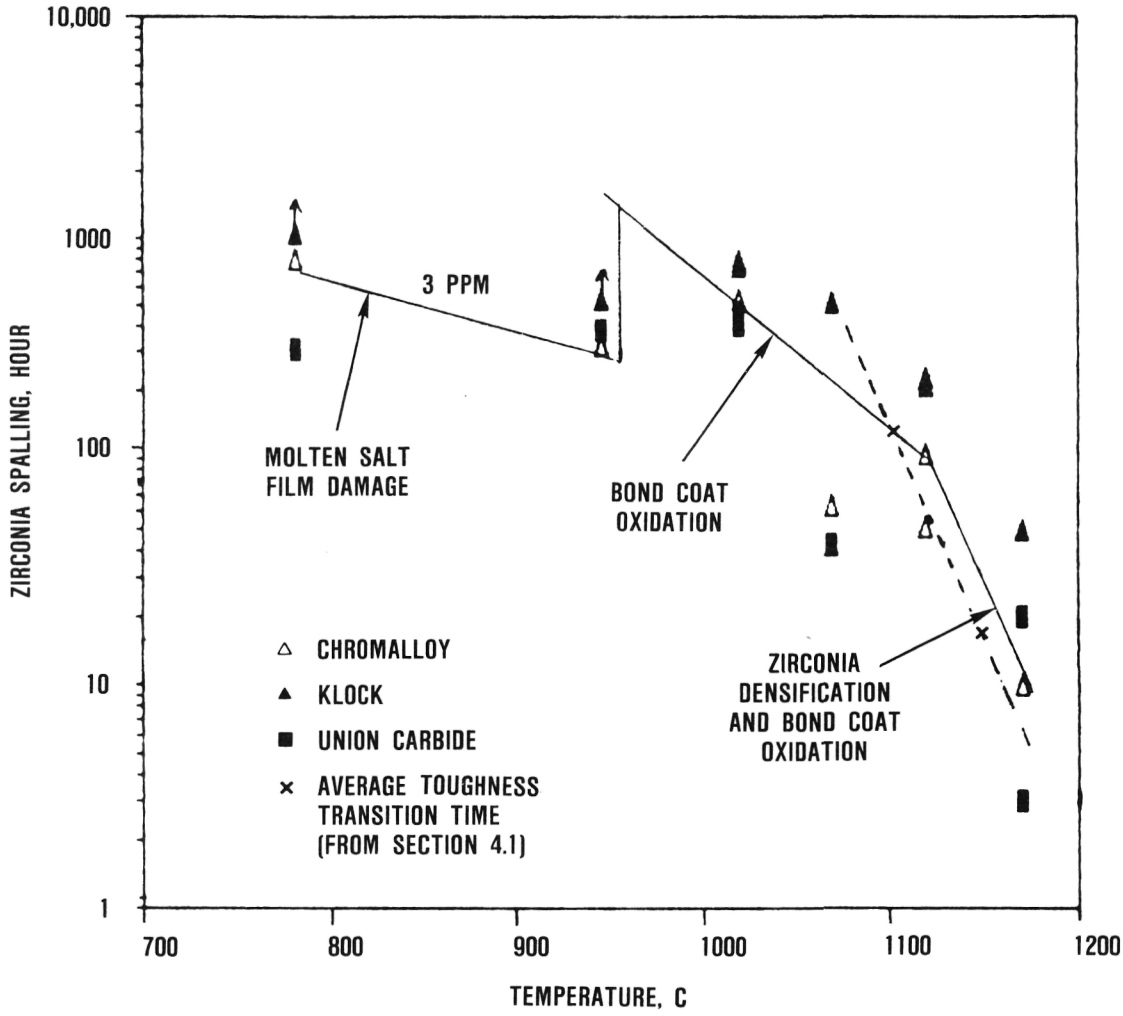

Figure 4-11. Three Degradation Modes Affect the Durability of Plasma-Sprayed TBC Systems.

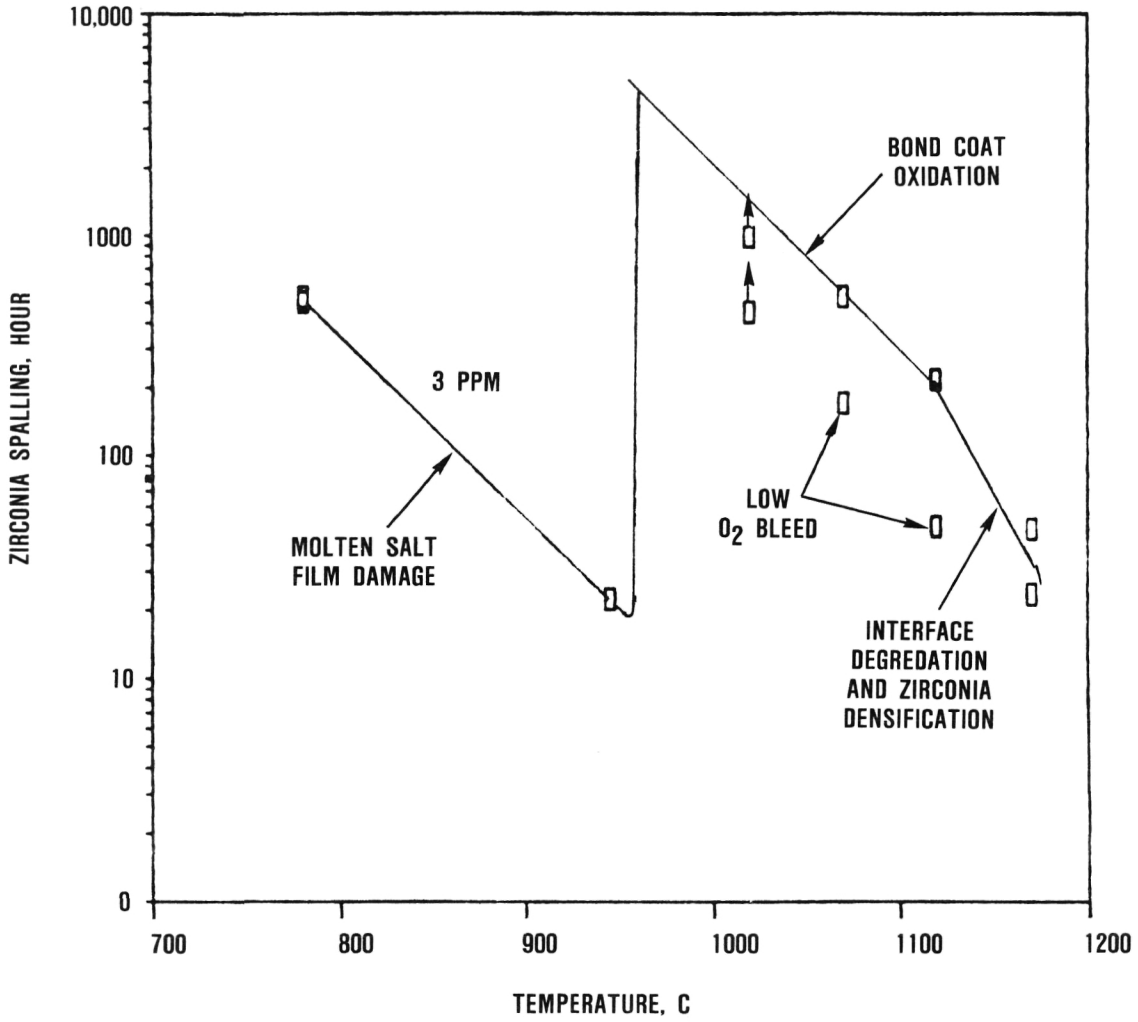

Figure 4-12. Three Degradation Modes Affect the Durability of Temescal's EB-PVD TBC System.

of cycle length on TBC life. Data from the 1020C tests with 4 and 27 minutes of hot time per cycle are shown graphically in Figure 4-13 and compared with 1100C data reported by Miller [4]. These data indicate that the shorter cycles result in a slightly reduced life over the temperature range of 1020 to 1100C. Sheffler and DeMasi [5] reported similar trends were observed over the interval of about 1100 to 1170C.

A typical aircraft engine mission cycle will have dwell periods of varying durations at several different temperatures; for example, a few minutes at take-off power, perhaps 10 minutes at climb power and 0.5 to 5 hours at cruise power. Therefore, in order to analyze burner rig data obtained at different cycle periods as well as predict TBC spalling for engine mission cycles of various lengths, the following cycle length correction factor was developed:

$$\text{Coating life}_{t_i} = (\text{Burner rig test life})\,(t_i^{0.25} + 0.181), \qquad (3)$$

where t_i is the increment of hot time in hours and the burner rig test life is for the 27 minutes hot and 3 minutes forced air cool cycle. The cycle period correction term equals one when there is 27 minutes of hot time per cycle.

Examination of the Chromalloy and Klock plasma sprayed coatings, which had lives greater than about 100 hours at the higher temperatures, confirmed the presence of significant bond coating oxidation at both the zirconia-bond coating interface and at internal porosity within the bond-coating (Figure 4-14). This figure also indicates that the lower aluminum content Union Carbide bond coating exhibited significant oxidation degradation at shorter times and lower temperatures. In contrast, TBCs that spalled after only a few hours of testing typically exhibited minimal oxidation degradation of the bond coating (Figure 4-15). This figure also indicates

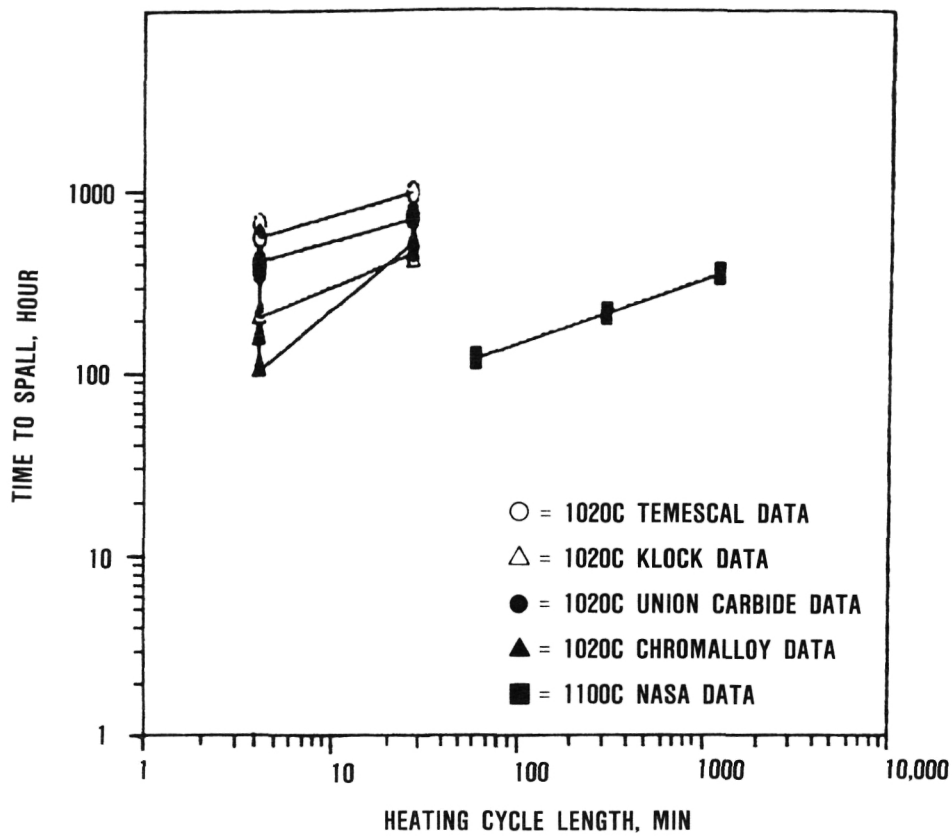

Figure 4-13. TBC Life Decreases with a Shorter Heating Cycle.

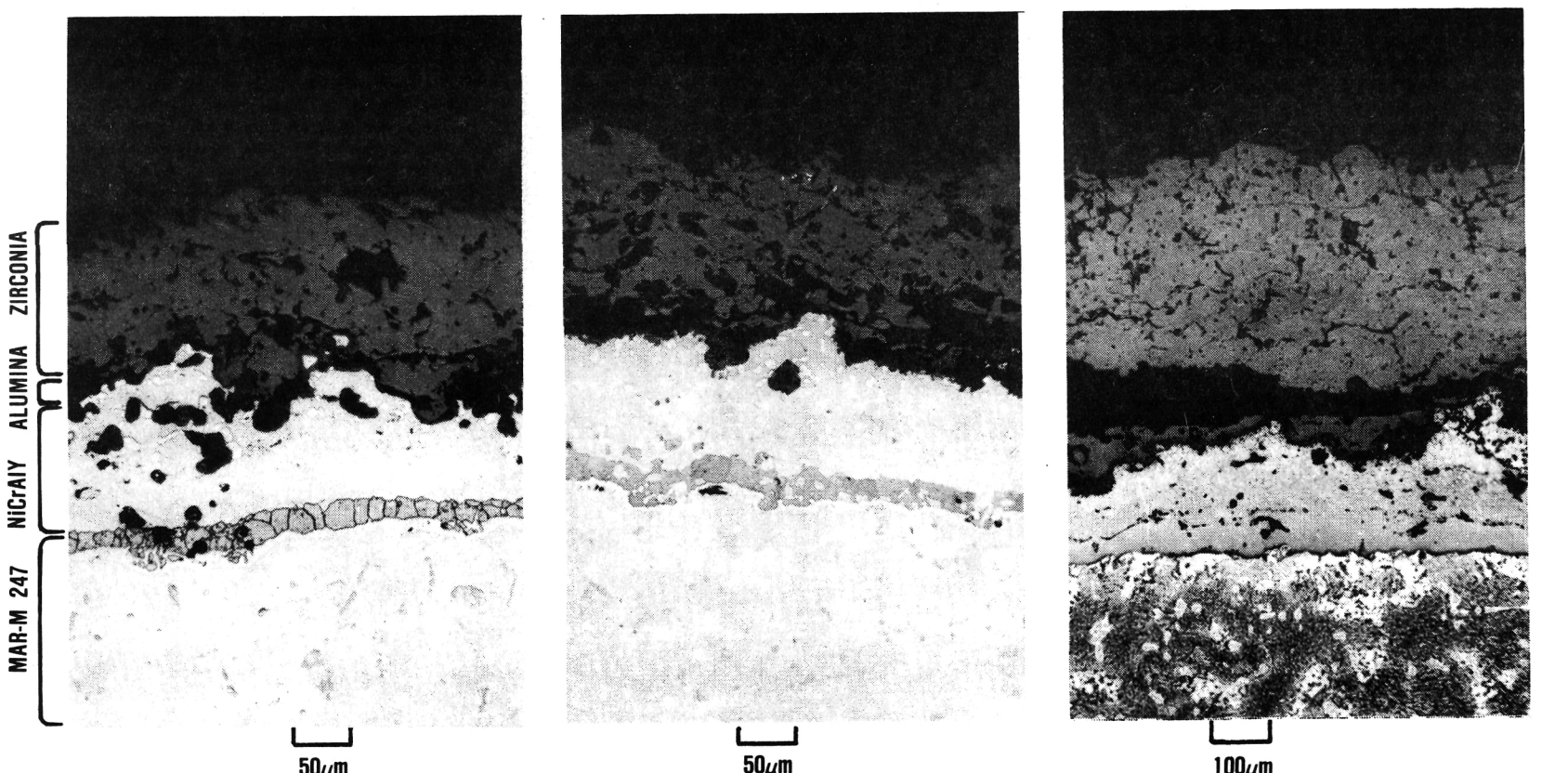

TIME IN TEST:	100 HOURS	218 HOURS	42 HOURS
COATING SOURCE:	CHROMALLOY	KLOCK	UNION CARBIDE
TEST TEMPERATURE:	1120C	1120C	1070C

Figure 4-14. Bond Coating Oxidation and Zirconia Densification Contribute to Plasma Sprayed TBC System Degradation During Burner Rig Tests.

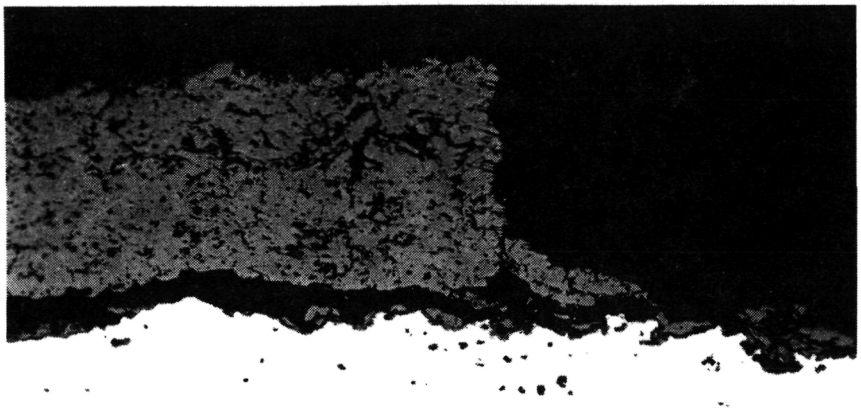

Figure 4-15. Zirconia Delamination from the Bond Coat is Caused by Crack Running Parallel to the ZrO_2/Bond Coat Interface, 100X. This Chromalloy Sample Spalled After 59.7 Hours in the 1070C Burner Rig Testing.

that propagation of delamination cracks typically occurred within the zirconia adjacent to the bond coating interface.

Densification of the zirconia by sintering shrinkage (Figure 4-14) was also observed. "Mud flat" type cracking was also observed in the zirconia coating layer during post-test visual examination, which is consistent with constrained sintering shrinkage. As noted in section 4.1, zirconia sintering densification was associated with a reduction in the zirconia toughness. This type of damage was observed in both short time and longer time tests conducted above about 1050C.

It was thought that a correlation should exist between the time to transition to the lower level of zirconia toughness and the burner rig data. Therefore, the burner rig data obtained above 1000C are compared in Figure 4-11 with the step transition times obtained from an analysis of toughness data in Figures 4-4 and 4-5. The correlation between zirconia toughness transition times and the burner rig data is good for the short life burner rig data points, where zirconia densification (mud flat cracking) was observed.

Comparison of the plasma sprayed and EB-PVD burner rig oxidation test data in Figures 4-11 and 4-12, respectively, indicated that both types of coatings have comparable lives above 1000C. Failure mechanisms were also similar for the NiCoCrAlY + 20 percent yttria stabilized zirconia EB-PVD TBC systems. As indicated in Figure 4-16, significant bond coating oxidation occurred in the longer tests. When significant oxidation occurred, the cracks associated with zirconia layer spalling propagated along the alumina scale or in the adjacent, relatively dense, non-columnar zirconia layer. Short time tests at 1170C indicated that the inner portion of the columnar zirconia had densified, which would increase stresses within the zirconia and the interface (Figure 4-17). This figure also

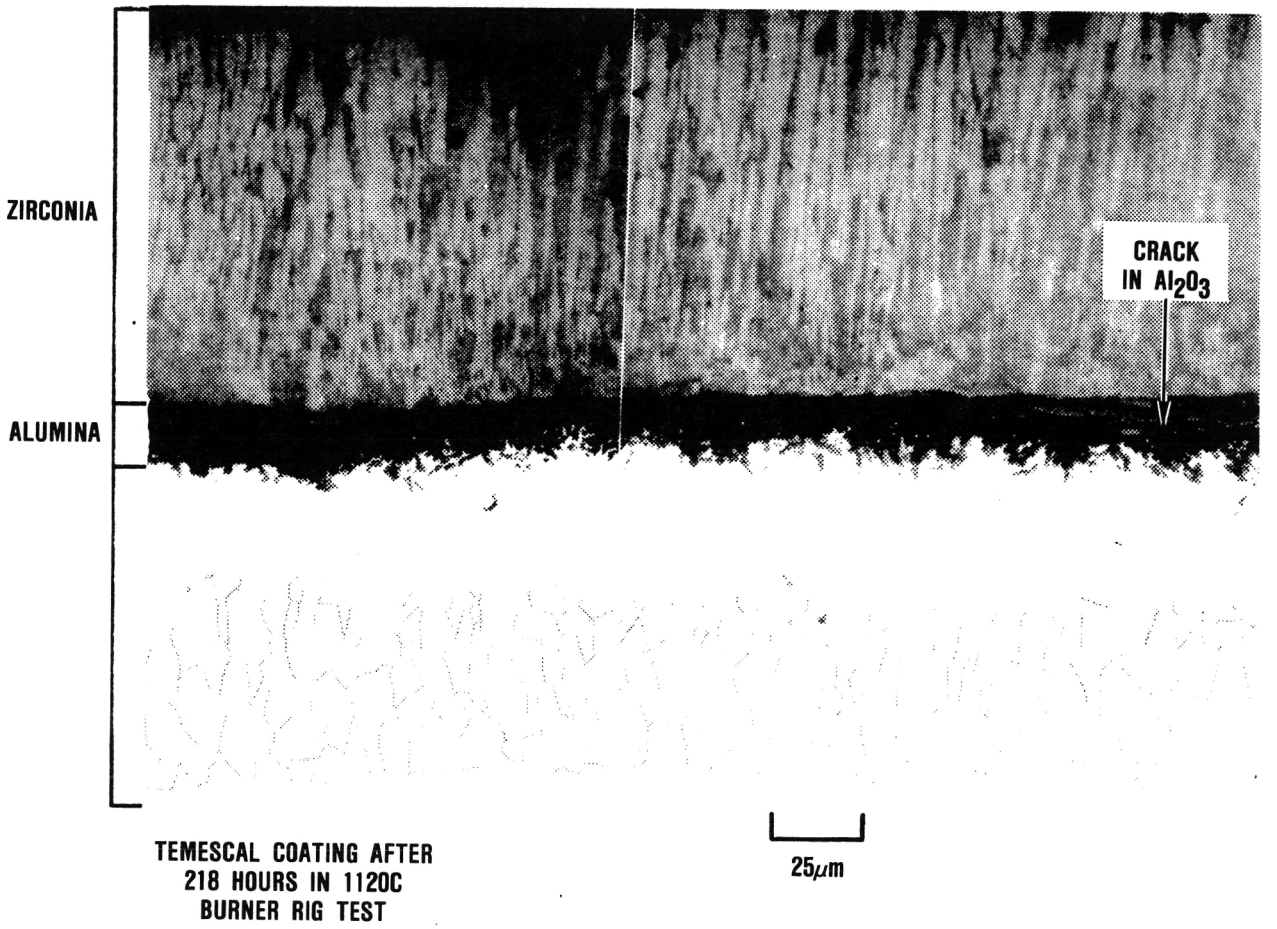

TEMESCAL COATING AFTER
218 HOURS IN 1120C
BURNER RIG TEST

Figure 4-16. Oxide Scale Growth Contributes to EB-PVD TBC Degradation.

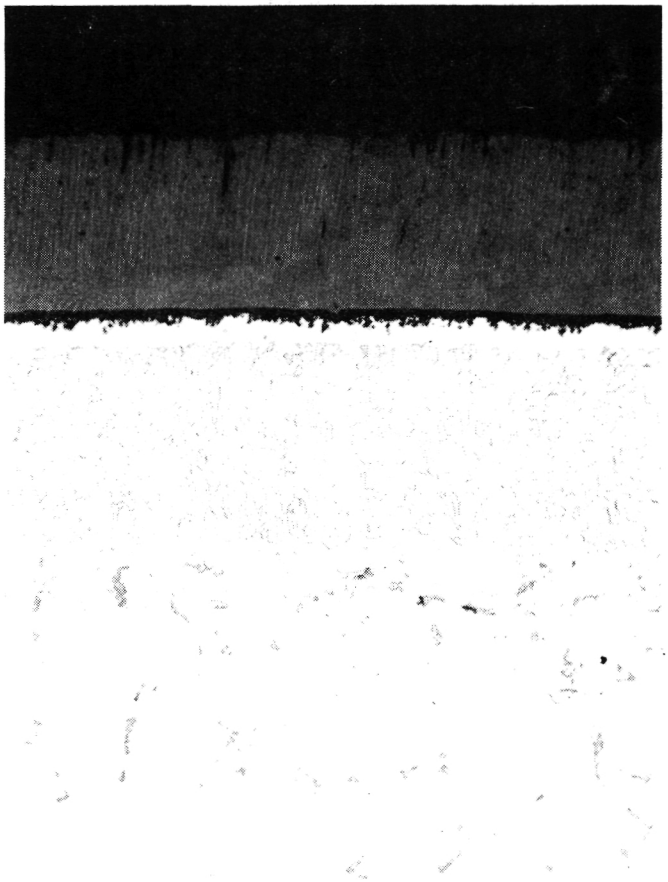

Figure 4-17. Inner Portion of EB-PVD Zirconia was Densified After 47 Hours in the 1170C Oxidation Test, 200X Magnification.

illustrates that bond coating oxidation was minimal for the short time failures.

In two instances, short time failures occurred at lower temperatures. A review of process records at Temescal indicated that these specimens had been coated at reduced oxygen bleed levels. It is thought that subsequent exposure of the oxygen deficient zirconia microstructure to high temperature air resulted in some volumetric expansion of the columnar grains, which reduced or eliminated the strain accommodating intercolumnar gaps and resulted in significantly increased coating stresses. This processing deficiency was subsequently eliminated. The two questionable data points are indicated in Figure 4-12.

In burner rig tests conducted at 945 and 780C with sea salt ingestion into the combustion air at 0.3 and 3 parts per million, reduced zirconia spalling lives were observed for both the plasma sprayed and EB-PVD systems as indicated in Figures 4-11 and 4-12.

Post-test microstructure analysis, however, indicates that the salt composition on the specimens may not be typical of salt deposits anticipated for an engine environment. The majority of the salt deposits were confined to the surface of the specimens. Energy dispersive x-ray (EDX) analysis of salt deposits on the surface of the burner rig specimens indicated that the primary constituents of the salt layer were S, Ca, and Na (Figure 4-18). Potassium and magnesium were also observed as secondary constituents. Silicon was also observed and was presumably a dust contaminant.

A comparison of the EDX pattern with the composition of the salt that was ingested (Table 4-1) indicates that chlorine is the major element that is absent. Chlorine would be lost from the salt deposit by evaporation of NaCl or by NaCl reaction with gaseous sulfur oxides to form sulfates and chlorine or HCl gas. The relatively

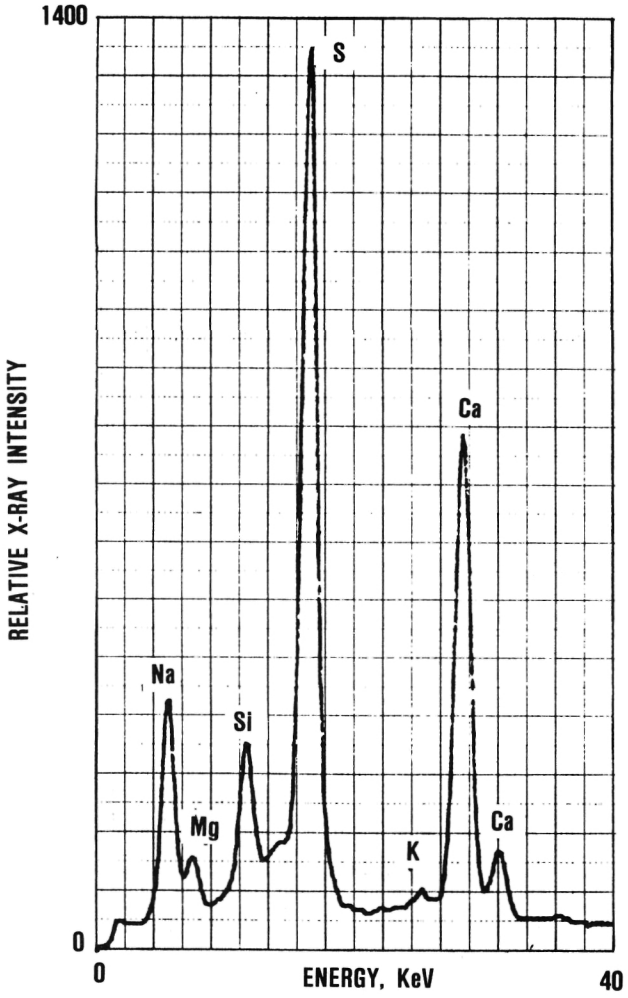

SEM PHOTO OF SALT DEPOSIT

Figure 4-18. The Chemistry of the Salt Deposits on the TBC Surface.

TABLE 4-1. COMPOSITION OF THE SEA SALT USED IN THE BURNER RIG TESTS

Element	Weight, %
Na	25.25
Mg	7.07
Ca	1.01
K	1.01
Cl	58.59
SO_4	7.07

small Na peak in Figure 4-18 may indicate that significant amounts of NaCl evaporated without reacting with gaseous sulfur oxides to form sulfates.

This result may be due to a low partial pressure of sulfur oxides in the burner rig test, relative to an engine. The sulfur content of the JP4 fuel used in these one atmosphere tests was 0.03 weight percent. In order to better simulate the SO_2 partial pressure conditions in a 10 atmosphere turbine, the sulfur content of fuel would need to be increased by a factor of ten to about 0.3 percent. Consequently, in the remaining tests requiring salt ingestion, SO_2 will be added to the combustion air at a level equivalent to 0.3 percent sulfur in the fuel. It is anticipated that this change will increase the amount of sodium sulfate present in the salt and increase the fluidity of the salt. (Salt deposits on the specimens did not appear to have been fully molten. The melting point of $CaSO_4$ is about 1300C.)

Fresh fracture surfaces were examined in the scanning electron microscope and x-ray dot maps for S and Ca, which exhibited the strongest peaks in surface salt deposits, were used to detect salt penetration into the zirconia microstructure. As expected, the open columnar microstructure of the EB-PVD zirconia was associated with the greatest amount of salt penetration. Less salt penetration was observed in the plasma sprayed zirconia systems at failure. It is thought that both types of TBC systems could be improved, with respect to inhibiting molten salt film damage, by densification of the zirconia surface.

4.4 Thermal Conductivity

Thermal conductivity is the critical design property of TBCs, which governs heat transfer into air-cooled turbine components. Component metal temperatures and thermal strains are dependent upon

the thermal conductivity of the zirconia layer. Therefore, to facilitate thermal and stress analyses of engine components, thermal conductivity of plasma sprayed and EB-PVD coatings was quantified in this program.

Testing was performed at Dynatech (Cambridge, MA) using the comparative method to determine thermal conductivity at 500, 800, and 1000C. The specimen geometry is shown in Figure 3-7. The substrate was instrumented with thermocouples and placed between two reference standards of identical geometry Figure 4-19. Each standard (heat meter) was instrumented with thermocouples at known fixed distances. The composite stack was fitted between an upper heater and lower heater of appropriate geometry and the complete system placed on a liquid cooled heat sink. A reproducible load was applied to the top of the system to ensure intimate contact between all components. A thermal guard tube which could be heated or cooled was placed around the system and the interspace and surroundings filled with an insulating powder.

The temperature drop across the coatings was obtained by extrapolating internal temperatures of the references and substrate to the surface on either side of the coatings.

By setting the top heater to a temperature higher than the lower heater, a temperature gradient was established in the stack. Radial heat loss was minimized by establishing a similar gradient in the guard tube. The system was allowed to reach equilibrium conditions after which successive readings of temperatures at various points were averaged and evaluated. From this data, heat flux was determined and specimen thermal conductivity calculated.

Thermal conductivity data for the Chromalloy and Klock plasma sprayed ytrria (8 weight percent) stabilized zirconia coatings and

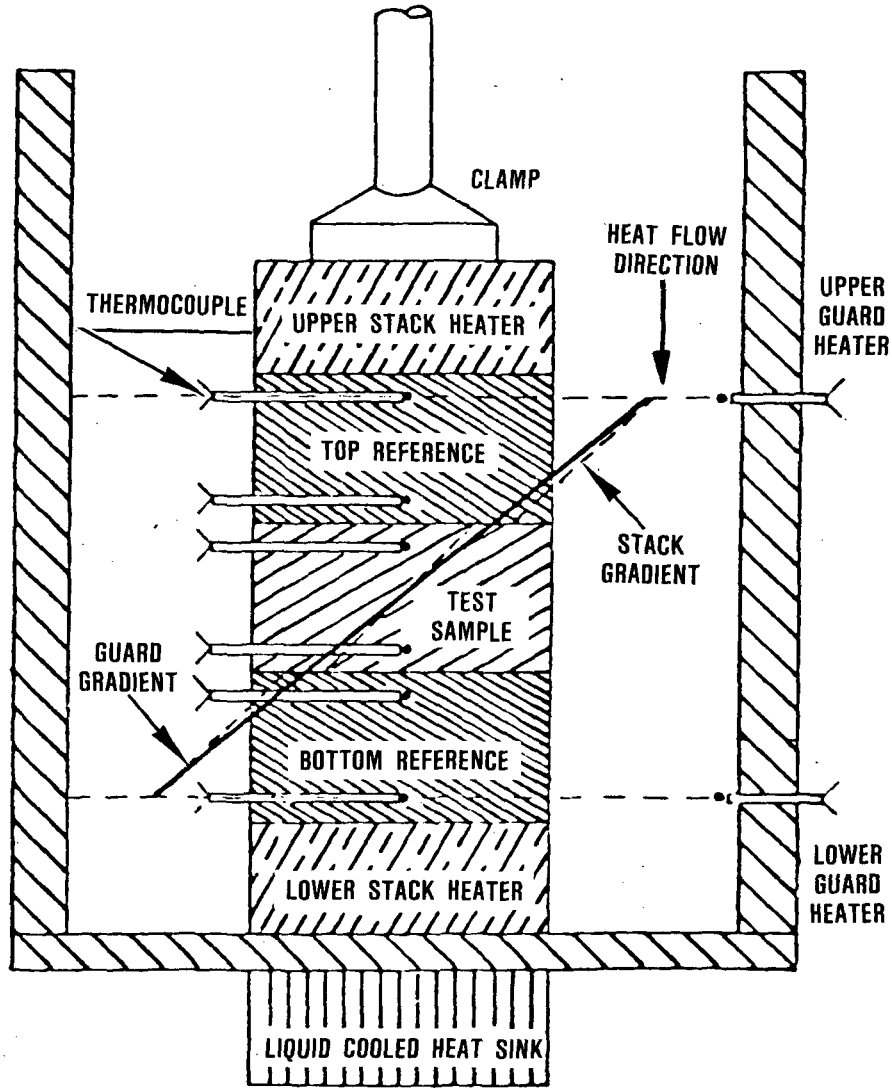

Figure 4-19. Schematic Diagram of Comparative Thermal Conductivity Test Stack.

Temescal EB-PVD yttria (20 weight percent) stabilized zirconia coating, provided in Figure 4-20 and Table 4-2, are in excellent agreement with published data for this coating from other NASA sponsored programs. This figure also indicates that the plasma sprayed and EB-PVD zirconias are about a factor of thirty lower than a typical superalloy, such as Mar-M 247 at about 1000C. Zirconia coatings evaluated in this program are also about a factor of 3 lower in conductivity than dense plasma sprayed zirconia after sintering at 2000C[6]; this result is attributed to the porosity and sub-critical microcracks within the microstructure.

TABLE 4-2. PLASMA SPRAYED AND EB-PVD ZIRCONIA COATINGS HAVE COMPARABLE THERMAL CONDUCTIVITY

	Thermal Conductivity, W/mK			
Sample	@ 500C (930F)	@ 800C (1470F)	@ 1000C (1832F)	Comments
T30H-1T	0.64	0.68	0.89	EB-PVD ZrO_2 from Temescal
T30H-3T	0.54	0.56	0.75	EB-PVD ZrO_2 from Temescal
K50H-1	0.58	0.59	0.78	Plasma-sprayed ZrO_2 from Klock
K50H-2	0.61	0.63	0.74	Plasma-sprayed ZrO_2 from Klock
C50H-1	0.67	0.69	--	Plasma-sprayed ZrO_2 from Chromally
C50H-2	0.68	0.69	--	Plasma-sprayed ZrO_2 from Chromally

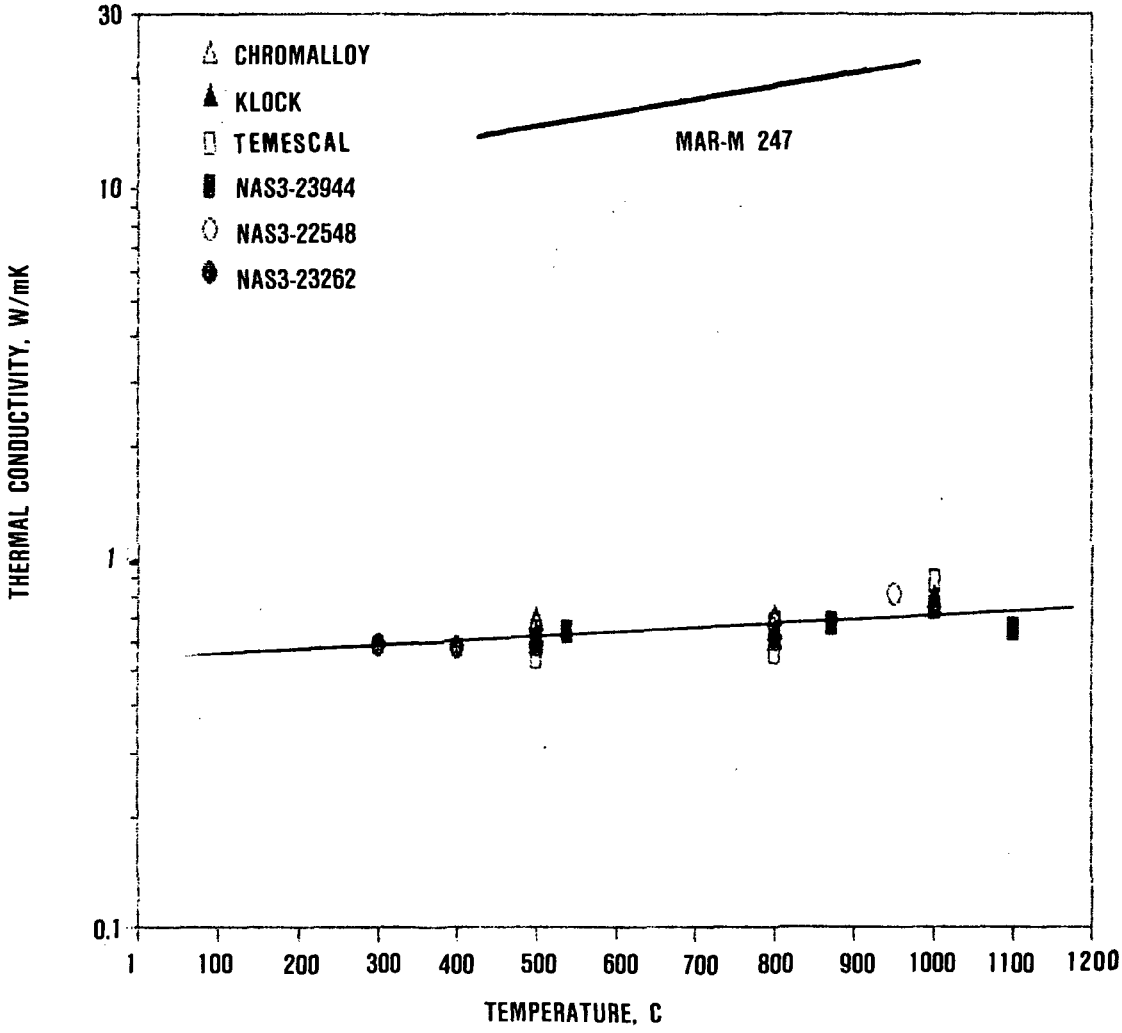

Figure 4-20. Thermal Conductivity Data for Plasma Sprayed Yttria (8 Weight Percent) Zirconia and EB-PVD Yttria (20 Weight Percent) Zirconia are in Excellent Agreement with Published Data.

4.5 Nondestructive Evaluation (NDE) Technologies

Effective exploitation of TBCs requires that critical materials properties be verified. The insulative capability of a TBC is dependent upon zirconia thickness and microstructure. Mechanical integrity of TBCs is dependent upon the microstructure of the coating and the size of critical flaws. Therefore, feasibility of using NDE technologies (eddy current, photothermal radiometric imaging and scanning photoacoustic microscopy) was assessed for potential to verify coating thickness and flaw sizes. Evaluation of these techniques is discussed in the following paragraphs.

4.5.1 Eddy Current Evaluation

An eddy current technique was used to successfully measure the thickness of the zirconia layer for both the plasma-sprayed TBC systems Chromalloy and Klock and Temescal's EB-PVD TBC system. Variations in the thickness of the ZrO_2 coating on the order of 25 to 50 μm (1 to 2 mils) are detectable. The results of this thickness determination study are shown in Figure 4-21. Five points were taken for each specimen along with air and the uncoated back of each specimen.

Insulative capabilities of TBCs on turbine components can, therefore, be established by using Eddy Current technology to verify zirconia thickness and using sample tabs to verify TBC microstructure.

4.5.2 Photothermal Radiometric Imaging

The experimental study of Photothermal Radiometric Imaging NDE technique was conducted by Dr. I. Kaufmann at Arizona State University. The experimental apparatus is illustrated schematically in Figure 4-22.

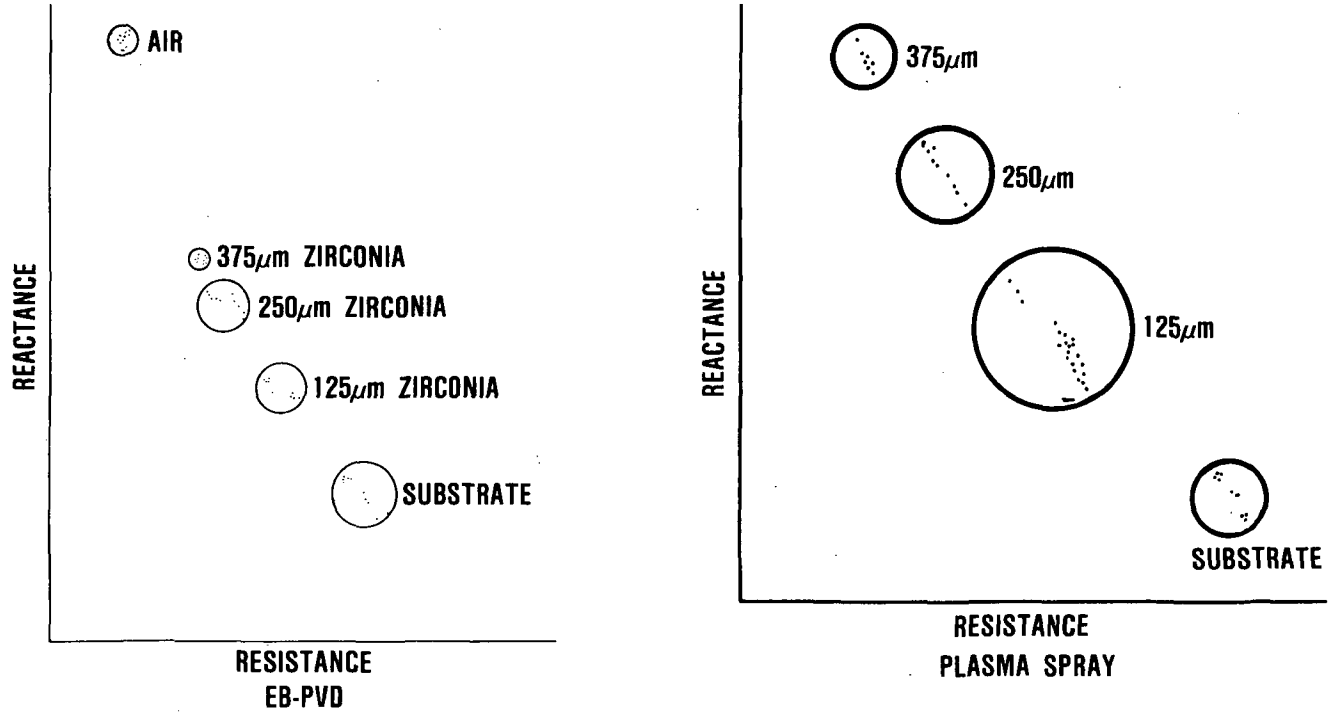

66-095-29

Figure 4-21. Eddy Current Inspections of EB-PVD and Plasma-Sprayed Zirconia Coatings are Comparable.

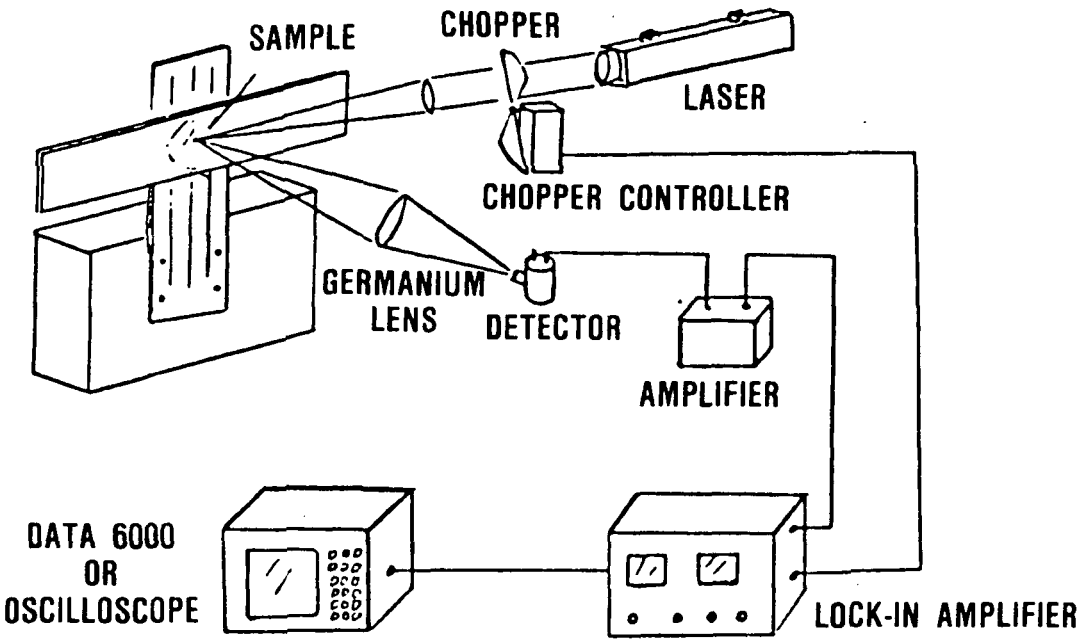

Figure 4-22. Photothermal Radiometric Imaging NDE Technique was Evaluated at Arizona State University.

Photothermal radiometric imaging was not successful in reliably detecting artificial flaws in either plasma sprayed or EB-PVD TBC systems. Specimens used for this study were identical to those used to measure cohesive and interfacial toughness (Figures 3-6 and 4-1). Flaw sizes varied from 0.5 to 6 mm in diameter. Limitations of the current technology in photoacoustic radiometric imaging are a slow scanning rate which requires a long inspection time and a low signal to noise ratio, which limits reliable flaw detection. Results of this investigation are described in detail in a separate report, which has been provided to the NASA program manager.

4.5.3 Scanning Photoacoustic Microscopy

The experimental study of the scanning photoacoustic microscopy NDE technique was conducted by Dr. R. Thomas at Wayne State University. A schematic diagram of the experimental set-up of this technique is shown in Figure 4-23.

Scanning photoacoustic microscopy was not successful in detecting artificial flaws in either plasma sprayed or EB-PVD TBC systems. Specimens used in this study were identical to those used to measure cohesive and interfacial toughness (Figures 3-6 and 4-1). Flaw sizes varied from 0.5 to 6 mm in diameter. Results of this investigation are described in detail in a separate report, which has been provided to the NASA program manager.

Until a viable NDE technique is developed to detect flaws within a TBC, it will be necessary to experimentally establish maximum effective flaw sizes using cohesive and adhesive strength specimens, which are coated concurrently with a batch of turbine components. This method of establishing flaw sizes was demonstrated in Section 4.1.

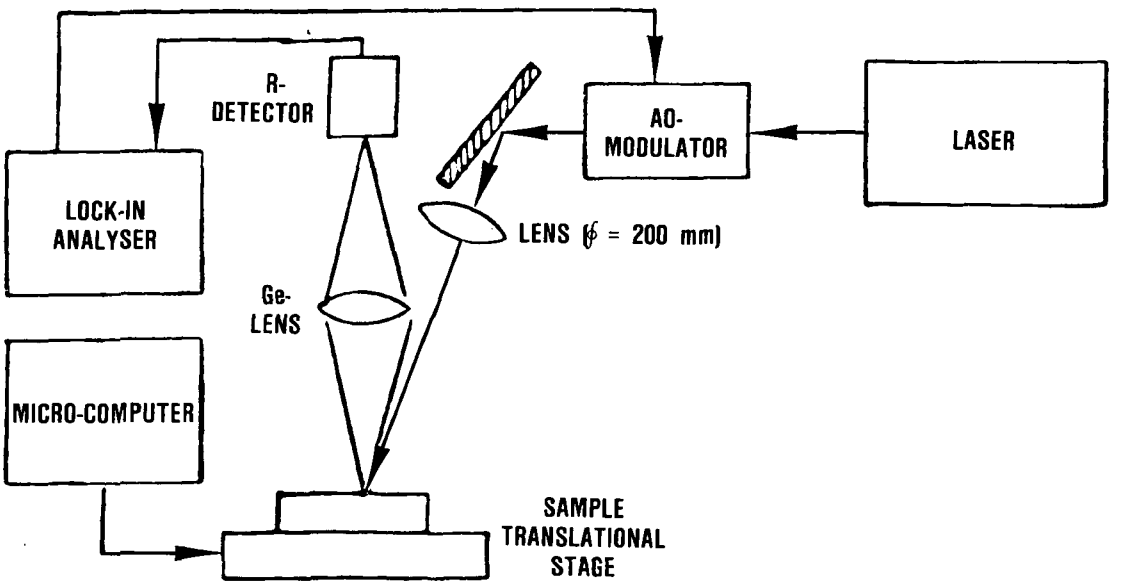

Figure 4-23. Scanning Photoacoustic Microscropy NDE Technique was Evaluated at Wayne State University.

5.0 MAJOR MODE LIFE PREDICTION MODEL DEVELOPMENT

5.1 Analysis Strategy

The overall objective of this task is to develop mechanistic mission-analysis-capable life prediction models for the predominant environmental and thermal/mechanical TBC failure modes for preliminary design analyses. Since the TBC must be considered early in the component design process in order to fully incorporate and exploit its benefits, an additional model goal was to drive the preliminary TBC life model with component thermal analysis data and simple snap acceleration-snap deceleration stress analysis data. This approach permits the designer to economically include TBCs into initial iterations of the blade and vane design process. More refined TBC analyses for final design lives are the subject of Phase 2.

A comprehensive strategy (Figure 5-1) to achieve this goal has been developed that includes the analyses of the TBC durability on both the TFE731-5 HP turbine blades and the burner rig test specimens. Due to the complex nature of the problems involved, the finite element method is deemed to be most effective in promoting the in-depth understanding of the essential overall thermal/mechanical behavior of the TBC systems as well as the interactions between the individual material regimes and the interfacial conditions in the TBC systems. This approach also interfaces efficiently with existing airfoil design methods.

For computational efficiencies, typical preliminary design (PD) finite element models were first constructed to analyze the bulk behavior of the TBC systems on the component or specimen. Critical locations, in terms of temperatures, stresses, and strains or their combinations, can be identified from these PD models. Refined submodels are then constructed for analysis of critical locations. Detailed thermomechanical and thermochemical behaviors of the TBC

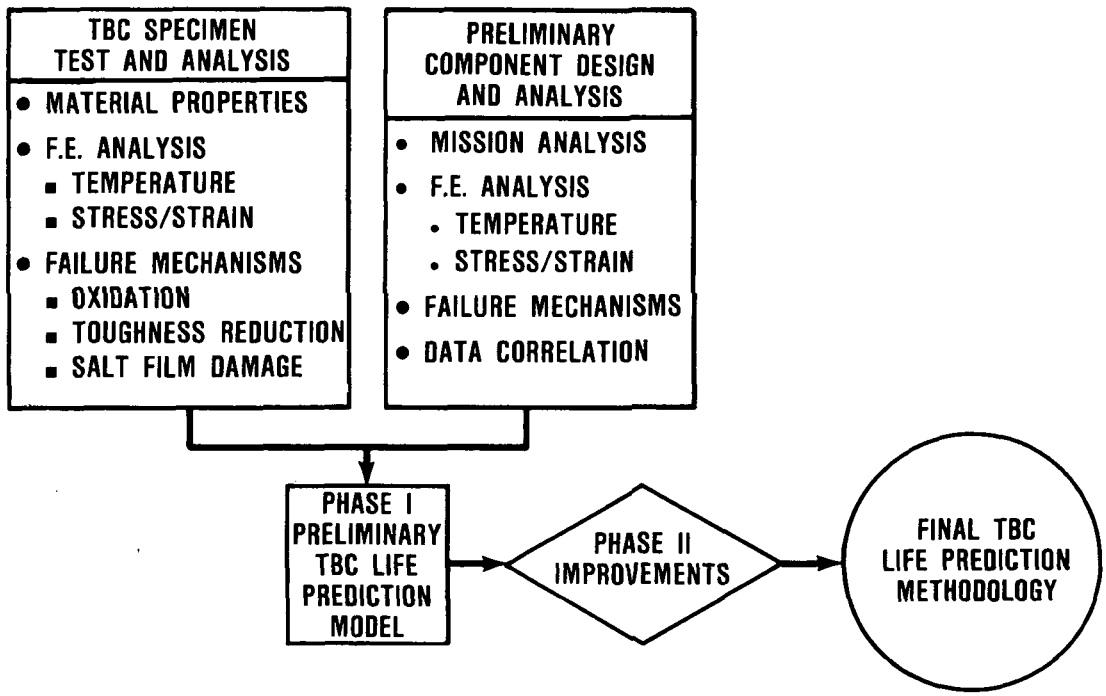

G6-100-149

Figure 5-1. NASA TBC Life Prediction Model Development Follows Two Paths.

systems and the interactions between the individual material regimes and the interfacial conditions can then be analyzed via these refined sub-models. Major analysis work in this program is being performed with ANSYS, a commercially available general purpose finite element code.

Computation of the oxidation life of a TBC system in the preliminary design model is driven by the component thermal analysis and engine power requirements during a mission cycle.

Molten salt film damage life is calculated using the component thermal analysis, engine power requirements during a mission, and aircraft altitude (salt ingestion).

Zirconia spalling associated with thermomechanical stresses is calculated based on the analysis of the snap-cycle thermal transients as well as the steady-state condition and the rotational loads in a mission cycle. Calculated snap-cycle interfacial tensile stresses and the largest pre-existing flaw diameter (determined by NDE or calculated from bond strength tests) are used to estimate a stress intensity factor that the coating must endure without spalling. As indicated in section 4.1, the fracture toughness of the zirconia or the bond coating-zirconia interface is dependent upon exposure temperature and time. Time and temperature dependent changes in the zirconia or interfacial toughness are calculated based on the thermal analysis results of the component and a linear cumulative damage model to account for variations in a mission cycle. Figure 5-2 is a schematic of the TBC life model that illustrates these three failure modes and the respective temperatures regimes at which these failure modes are likely to occur.

For preliminary component design analyses (Phase I), TBC lives are being independently calculated for three operative damage modes:

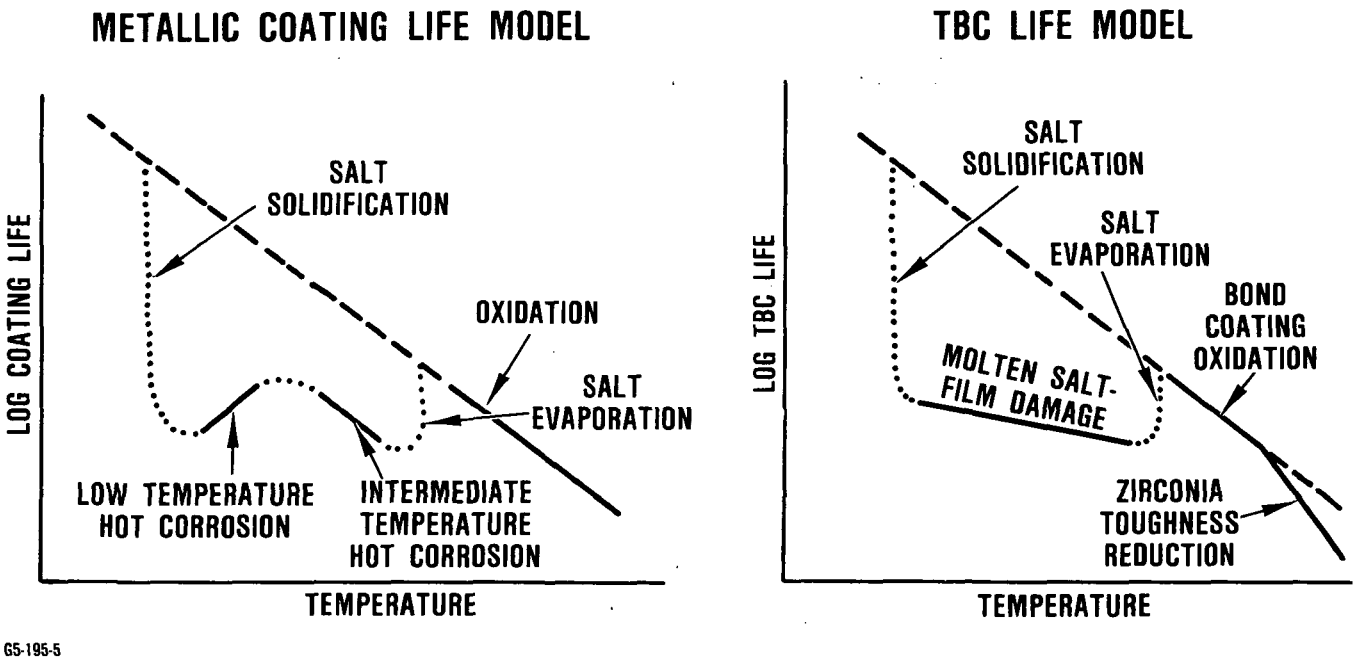

Figure 5-2. TBC Life Model Development is Facilitated by Metallic Coating Life Model.

- o bond coating oxidation
- o molten salt film damage, and
- o thermomechanical stress induced spalling.

Figure 5-3 illustrates parameters that affect each of these three major failure modes.

The preliminary design TBC life will be assessed via a linear damage rule, composed of damages from these three modes during each of the mission cycles, assuming no interactions between these failure modes; that is

$$\text{Life} = [(\text{Life}_{oxid})^{-1} + (\text{Life}_{salt})^{-1} + (\text{Life}_{stress})^{-1}]^{-1}$$

However, the refined sub-models are being constructed to be sufficiently flexible and detailed to analyze the interactions between these models. Subsequent improvements in Phase 2 of the program will incorporate failure mechanism interactions into the life prediction model.

5.2 Burner Rig Specimen Finite Element Analysis

Due to the geometric simplicity, the burner rig specimen is the preferred means by which statistically significant TBC failure data can be economically generated. It is also the more efficient means with which the mechanistic TBC life prediction model can be developed.

Operative temperature ranges for the materials models used in TBC life analyses are illustrated schematically in Figure 5-2 and quantitatively in Figures 4-11 and 4-12 for plasma sprayed and EB-PVD systems, respectively. Figure 5-2 also emphasizes the similarities and differences between the TBC life model and GTEC's oxidation/hot corrosion life model for metallic coatings.

TBC DEGRADATION RATE = F_1 (MECHANICAL) + F_2 (OXIDATION) + F_3 (SALT DEPOSITION)

F_1 (MECHANICAL)
- COATING STRESSES
- TEMPERATURE
- MATERIAL SYSTEM
  - K_{IC}
  - FLAW SIZE
  - ELASTIC MODULUS
  - SPALLING STRAIN

F_2 (OXIDATION)
- TEMPERATURE
- TIME
- MATERIALS SYSTEM

F_3 (SALT DEPOSITION)
- ALTITUDE (SALT INGESTION)
- TURBINE PRESSURE
- SALT EVAPORATION
- SALT SOLIDIFICATION
- TEMPERATURE
- GAS VELOCITY
- AIRCRAFT LOCATION
- MATERIALS SYSTEM

G5-195-3

Figure 5-3. TBC Life is a Function of Engine, Mission and Materials System Parameters.

Figure 5-4 illustrates the logical sequence that the finite element analysis of the burner rig specimen is following to achieve a preliminary TBC life prediction model.

A two-dimension (2-D) plane-strain finite element model is being built, which contains the metallic substrate (MAR-M247), bond coating and zirconia layers. Thermal and stress/strain analyses are being performed with this model. Thermal boundary conditions are being generated based on measured specimen temperatures.

Refined sub-models are being constructed to further analyze the detailed thermomechanical behavior within each of the material regimes, using the results from the 2-D model as the input. The sub-models are detailed enough and sufficiently flexible to analyze the interactions between the material regimes and the influence of oxidation effects on stresses. Figure 5-5 is a schematic representation of the burner rig specimen finite element model.

5.3 TFE731 HP Turbine Blade Finite Element Analysis

To demonstrate the applicability of the TBC life model for turbine airfoil preliminary design analysis, a TBCed HP turbine blade in a TFE731 turbofan engine is being analyzed for a factory engine snap-acceleration snap-deceleration test cycle. (As described in Section 6, program TBCs have been applied to this blade and are being engine tested to provide engine validation data.)

Analysis of this airfoil is proceeding according to the preliminary design strategy described in Section 5.1. Thus far, 2-D and 3-D finite element preliminary design models have been constructed. These models are being used to conduct thermal as well as stress/strain analyses. Results are being used to identify critical locations.

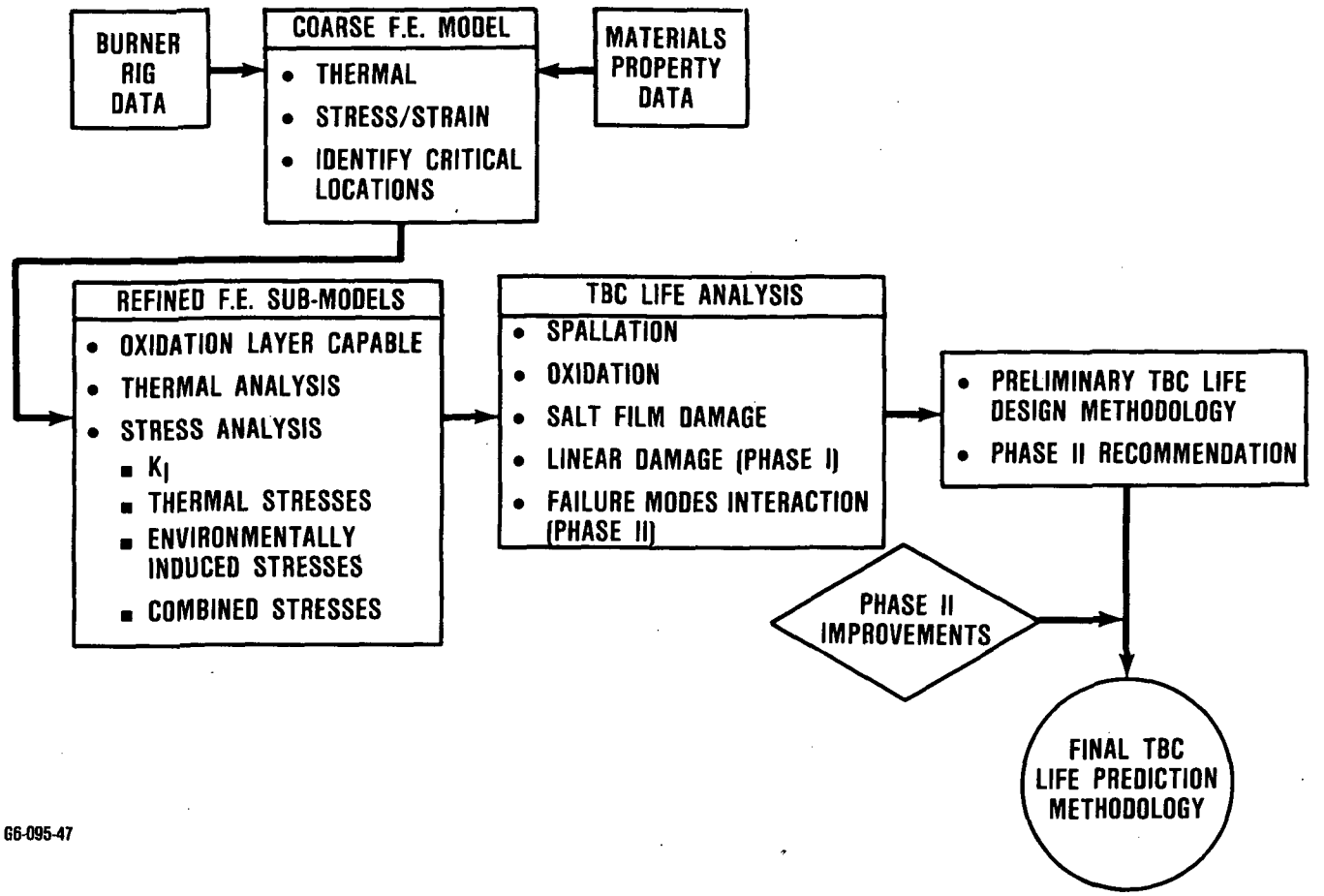

Figure 5-4. Burner Rig Specimen TBC Life Model is Being Developed.

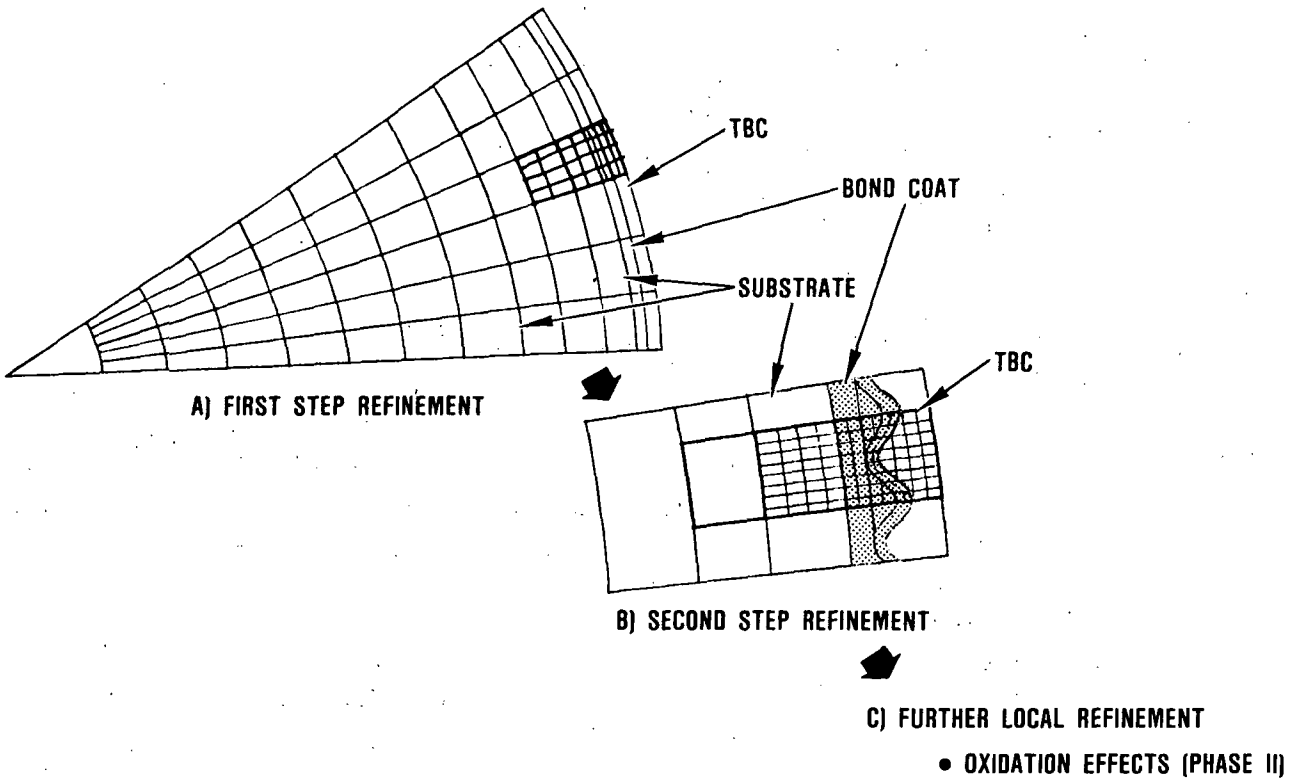

Figure 5-5. Burner Rig Finite Element Model will Evolve in the Following Steps.

Refined sub-models are being built for the critical locations identified from the overall models. These sub-models will have the capability to analyze the effects of oxidation. Results obtained from the sub-models will be used to assess the damage from each of the major TBC failure modes, namely, the bond coat oxidation, the salt film damage, and the thermomechanical stress-induced failures. A linear cumulative damage approach will be taken to predict TBC life in Phase I. Interactions between the major failure modes will be subsequently incorporated into the detailed design model in Phase II. Figure 5-6 illustrates the overall approach of the finite-element analysis work of the TFE731-5 HP turbine blades.

Steady-state thermal and stress analysis of the TBC coated blade have been performed for the engine rated condition. The snap-cycle stress analysis is in progress for TBCed blades.

The 2-D and 3-D preliminary design finite element models for the airfoil are provided in Figures 5-7 and 5-8. Figures 5-9 and 5-10 are some of the sample results of the steady-state temperature distributions at the mid-span section of the blade at the rated condition of the engine, with a TBC thickness of 125 μm (0.005 inch). There is a 40 to 50C (70F to 90F) drop across the TBC layer at the various locations of the sectional profile.

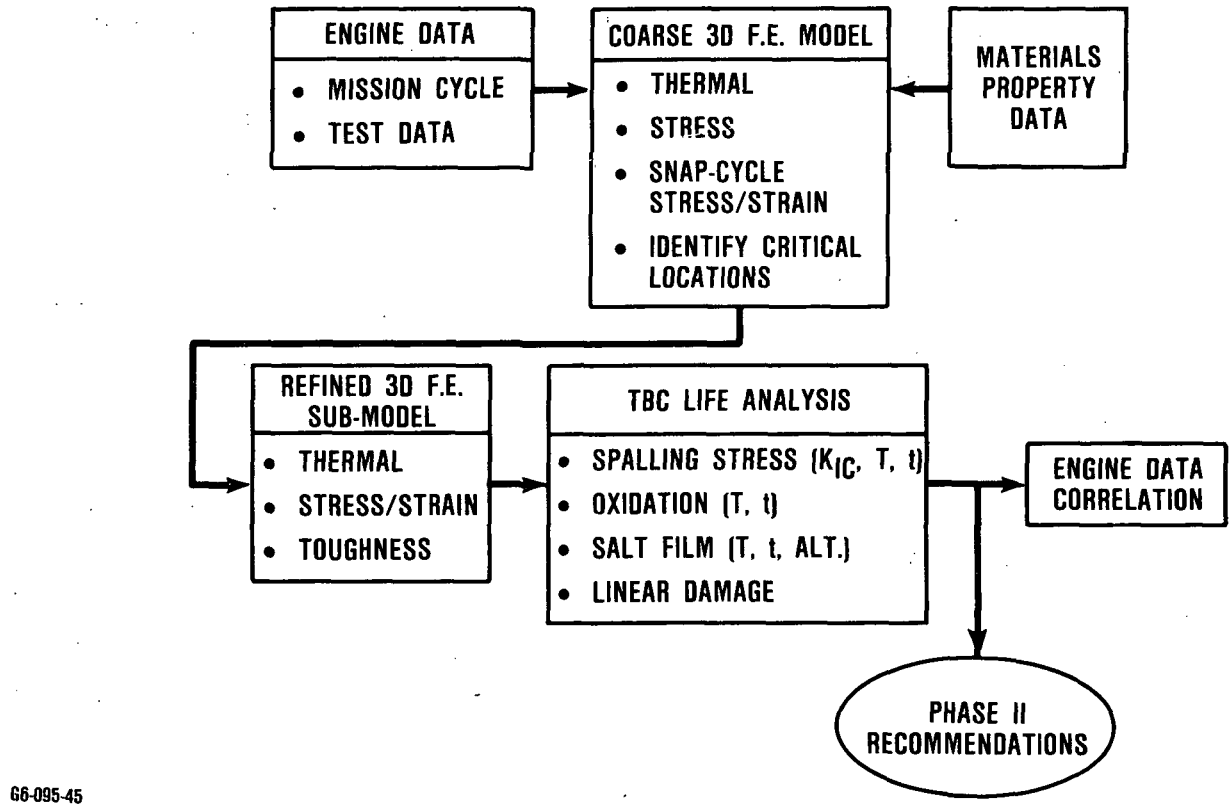

Figure 5-6. Three TBC Damage Modes are Evaluated in TFE731 Blade Analysis.

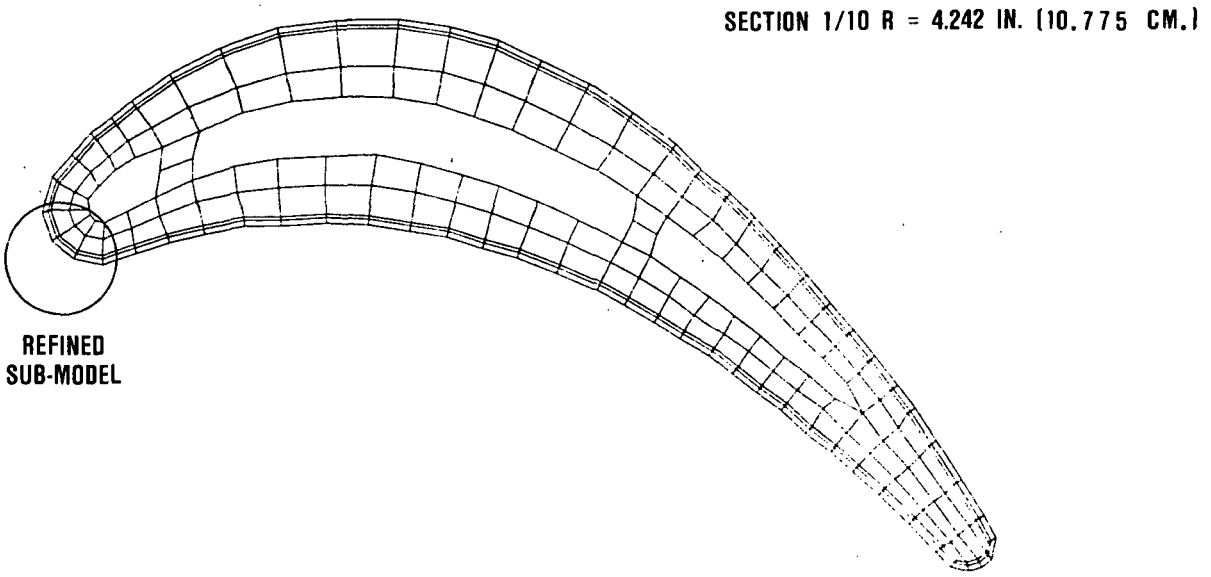

Figure 5-7. TFE731 HPT Blade F.E. Model Incorporates Bond Coating and Zirconia Layers.

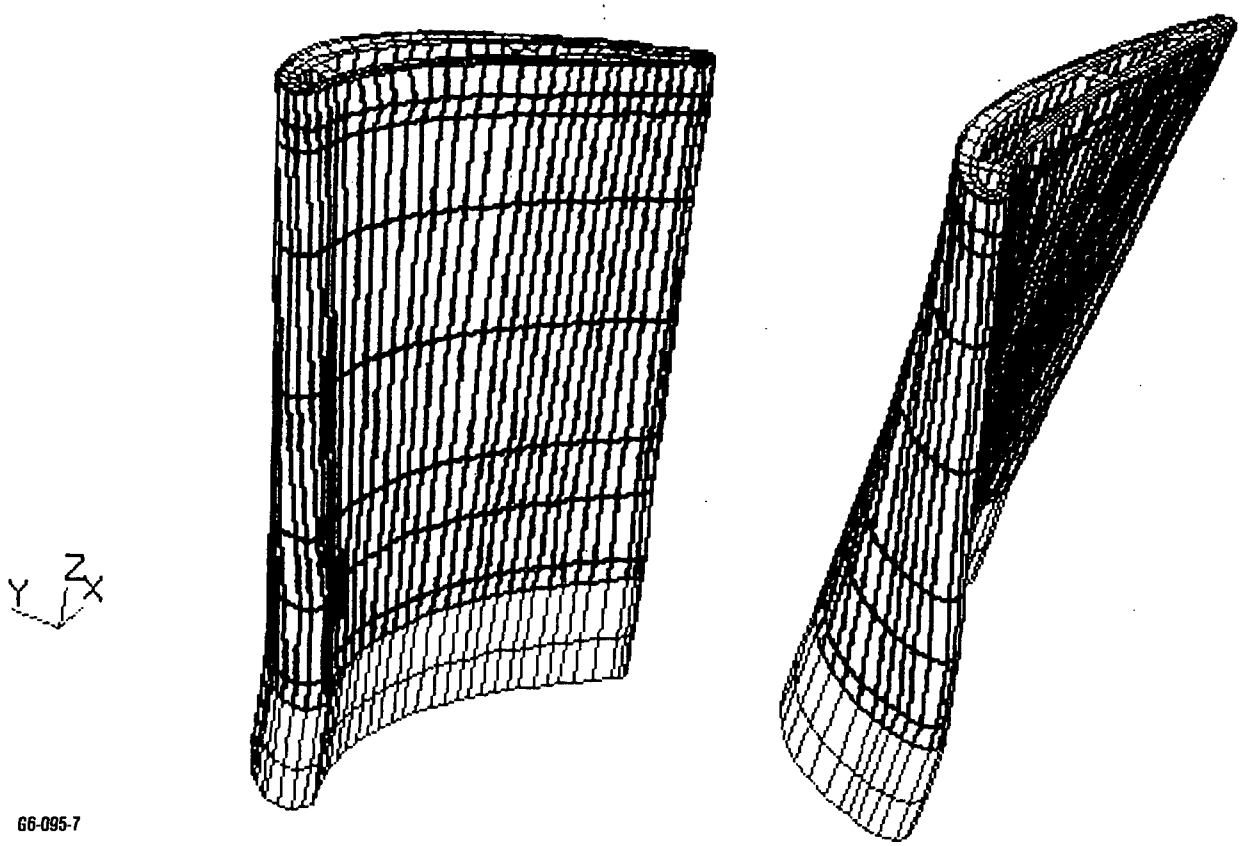

Figure 5-8. TFE731 HPT Blade 3-D F.E. Model Incorporates TBC.

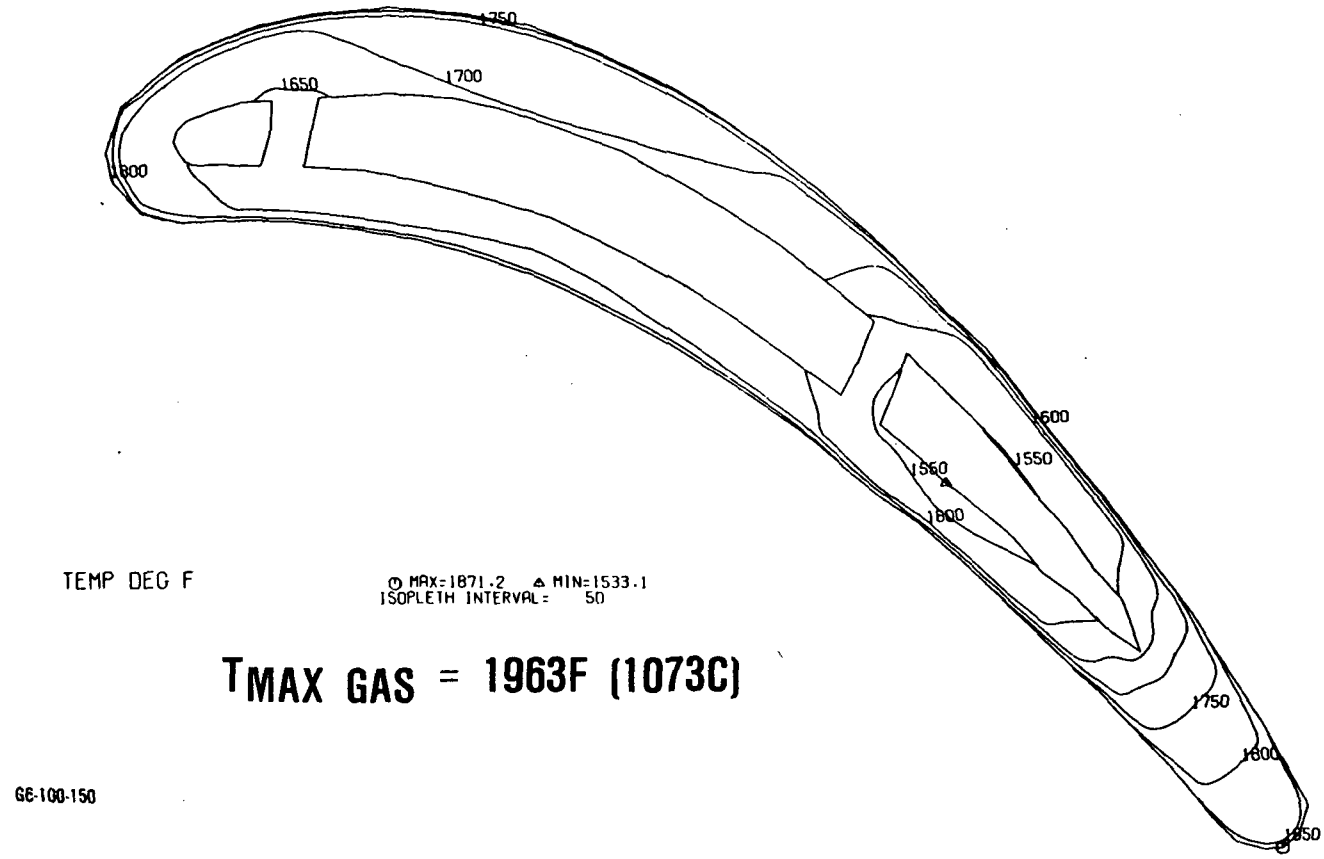

Figure 5-9. Thermal Analysis of TBC-Coated Blade has been Conducted.

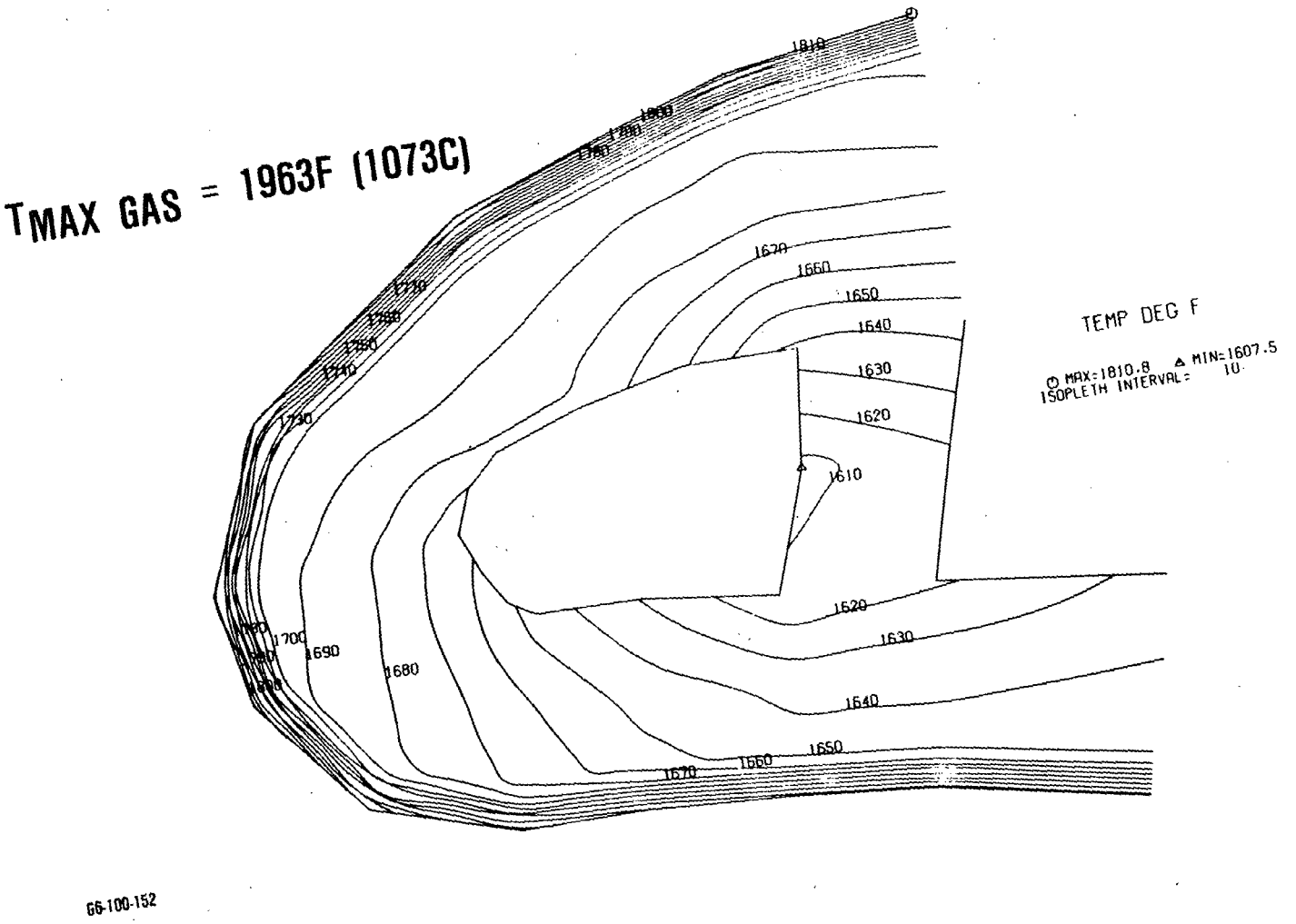

Figure 5-10. Thermal Analysis of TBC-Coated Blade has been Conducted.

6.0 ENGINE TEST

High pressure turbine blades were coated with the program TBC systems applied by Chromalloy, Klock, and Temescal, and are being "piggyback" tested in a TFE731 turbofan test engine. Data from this test is intended to provide data to verify the TBC life prediction model.

The Chromalloy and Temescal applied TBC systems have now accumulated 75 hours of predominantly snap-cycle testing and are in good condition. In contrast, the Klock applied TBC system exhibited leading edge spalling after 67 hours of testing (Figure 6-1) and were removed for metallographic evaluation.

Posttest analysis of the failed Klock TBC system on the TFE731-5 HP turbine blades revealed that a surface deposit wicked into the strain accommodating porosity and microcracks and densified the zirconia coating (see Figure 6-2). Densification of the zirconia increases both the elastic modulus and stresses within the zirconia layer. This deposit on the blades was rich in silicon, calcium, and aluminum. The chemical composition of the deposit is similar to a sample of cement or dust collected near the test cell (see Figure 6-3). This indicates that deposits on the TBC are not representative of typical aircraft propulsion engine environments.

Additional engine testing of the Chromalloy and Temescal TBCed blades is continuing.

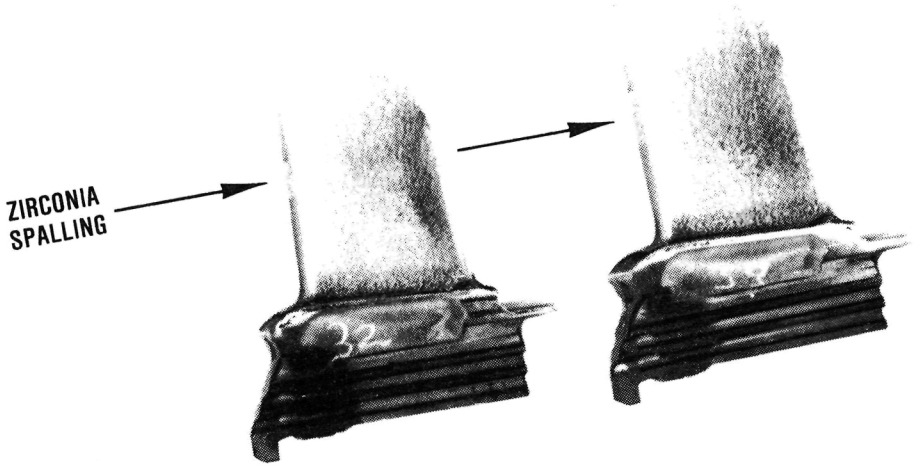

Figure 6-1. Zirconia Layer of Klock TBC System Spalled in the Center of the Leading Edge of High Pressure Turbine Blades of a TFE731 Engine Test.

200X

Figure 6-2. Zirconia Adjacent to the Surface Deposits was Densified on Klock Coated TFE731-5 HP Turbine Blades.

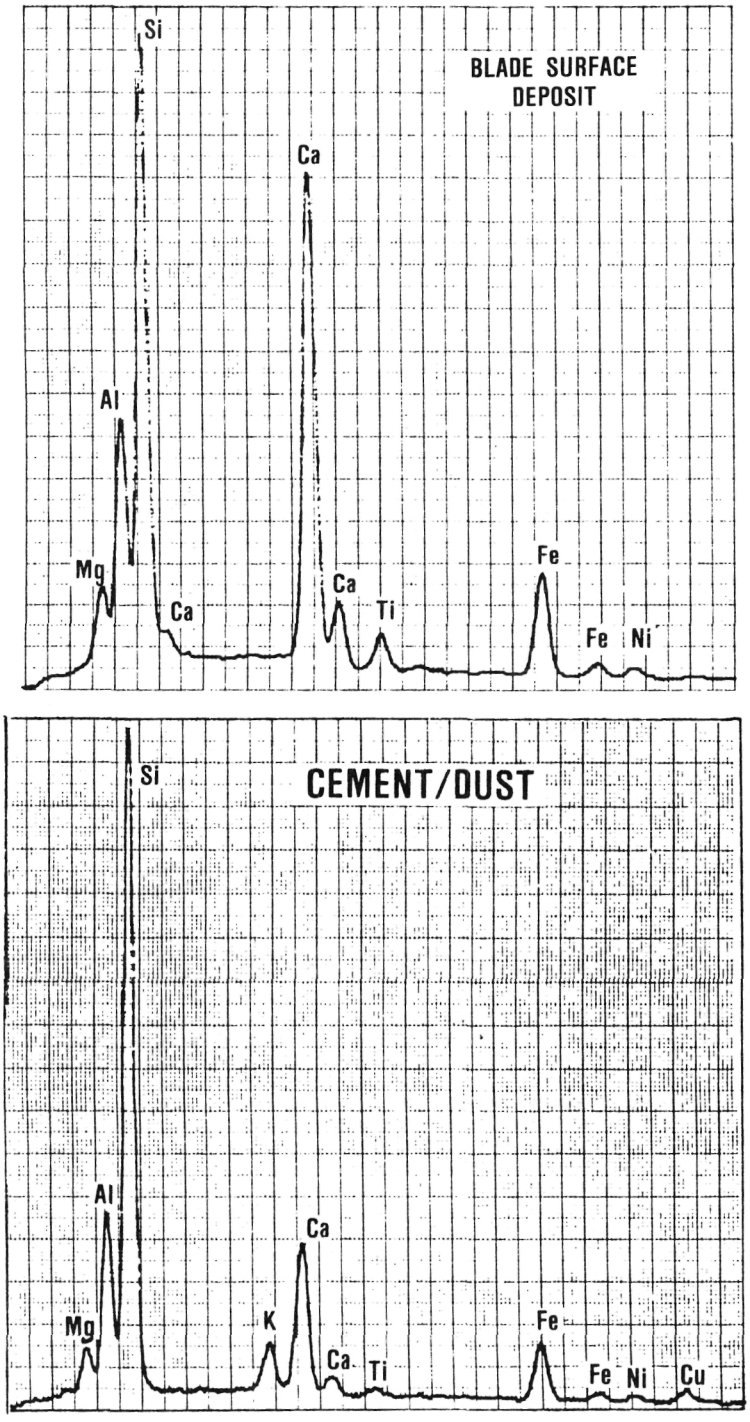

Figure 6-3. Chemical Composition of Blade Surface Deposit was Similar to a Sample of Cement or Dust Collected Near GTEC Test Cell.

7.0 CONCLUSIONS

During the second year of this program, GTEC has made significant progress in the development of life prediction methods for TBCed turbine airfoils. The status of key program elements are summarized below;

- Mission dependent TBC life models are being developed
- Three operative failure modes are being modeled in Phase I
- Life models are being developed for plasma sprayed and EB-PVD TBCs
- Life models are calibrated for commercially applied TBC systems from Chromalloy, Klock, Union Carbide and Temescal
- Affordable tests have been developed to calibrate thermomechanical and thermochemical TBC life models
- Efficient preliminary design TBC life prediction models are being developed and demonstrated for TFE731 turbine blades
- Turbofan testing is in progress to validate TBC life predictions.

REFERENCES

1. T.E. Strangman and J. Neumann, "Thermal Barrier Coating Life Prediction Model Development - First Annual Report," NASA CR-175002, 1985.

2. K.D. Sheffler, R.A. Graziani, and G.C. Sinko, "JT9D Thermal Barrier Coated Vanes," NASA CR-167964, 1982.

3. K.D. Sheffler and J.T. DeMasi, "Thermal Barrier Coating Life Prediction Model Development - First Annual Report," NASA CR-175087, 1985.

4. R.A. Miller, "An Oxidation Based Model for Thermal Barrier Coating Life," J. American Ceramic Society, 67 (1984) 517-521.

5. J.T. DeMasi, "Thermal Barrier Coating Life Prediction Model Development," P. 445-455 in Turbine Engine Hot Section Technology 1985, NASA CP 2405, 1985.

6. K.E. Wilkes and J.F. Lagedrost, "Thermophysical Properties of Plasma Sprayed Coatings," NASA CR-121144, 1973.

DISTRIBUTION LIST

D. L. Alger (301-2)
NASA Lewis Research Center
21000 Brookpark Road
Cleveland, OH 44135

L. F. Aprigliano
D. Taylor Shipyard
R&D Center
Annapolis, MD 21402

M. M. Bailey (77-6)
NASA Lewis Research Center
21000 Brookpark Road
Cleveland, OH 44135

Michael Bak (5-16)
Williams International
P.O. Box 200
Walled Lake, MI 48088

H. Beale
Applied Coatings, Inc.
775 Kaderly Drive
Columbus, OH 43228

Robert Beck
Teledyne - CAE
1330 Laskey Road
Toledo, OH 43612

Biliyar N. Bhat (EH-23)
NASA Marshall Space
Flight Center
Huntsville, AL 35812

Donald H. Boone
Naval Post-Graduate School
Dept. of Mechanical Engineering
Code 69BL
Monterey, CA 93943-5100

David Bott
Muscle Shouls Mineral Company
1202 East 2nd Street
Muscle Shoals, AL 35661

R. J. Bratton
Westinghouse Electric R&D
1310 Buelah Road
Pittsburgh, PA 15235

Sherman D. Brown
Chemical Engineering Dept.
University of Illinois
Urbana, IL 61801

Walter Bryzik (RGRD)
U.S. Army Tank-Auto. Command
Diesel Engine Research RMSTA
Warren, MI 48397

R. F. Bunshah
University of California
6532 Boelter Hall
Los Angeles, CA 90024

George C. Chang (MC 219)
Cleveland State University
Cleveland, OH 44115

Jerry Clifford
U.S. Army Applied Tech. Lab.
SAVDL-ATL-ATP
Fort Eustis, VA 23604

Dave Clingman
Detroit Diesel Allison - GMC
Engineering Operations
Indianapolis, IN 46206

DISTRIBUTION LIST CONTINUED

Arthur Cohn
E P R I
3412 Hillview Avenue
Palo Alto, CA 94303

Thomas A. Cruse
Southwest Research Institute
P.O. Box 28510
San Antonio, TX 78284

Keith Duframe
Battelle Labs.
Columbus, OH 43216

Mrityunjoy Dutta
U.S. Army AMSAV-EAS
4300 Goodfellow Blvd.
St. Louis, MO 63120

D. S. Engleby
Naval Air Rework Facility
Mail Drop 9, Code 017
Cherry Point, NC 28533

John Fairbanks (FE-22)
Department of Energy
Office of Fossil Energy
Washington, DC 20545

N. Geyer
AFWAL/MLLM
Wright Patterson AFB
Dayton, OH 45433

J. W. Glatz
NAPTC R&D Division
Naval Air Prop. Test Center
Trenton, NJ 08628

G. W. Goward
Coatings Technology Corp.
2 Commercial Street
Branford, CT 06405

M. A. Greenfield (RM)
NASA Headquarters
600 Independence Avenue
Washington, DC 20546

S. J. Grisaffe (49-1)
NASA Lewis Research Center
21000 Brookpark Road
Cleveland, OH 44135

D. K. Gupta
Pratt & Whitney Aircraft
400 Main Street
E. Hartford, CT 06108

William K. Halman
Temescal
2850 Seventh Street
Berkeley, CA 94710

D. Hanink
Detroit Diesel Allison-GMC
Engineering Operations
Indianapolis, IN 46206

Doug Harris
APS - Materials Inc.
153 Walbrook
Dayton, OH 45405

Harold Herman
Argonne National Lab.
9700 South Cass Avenue
Argonne, IL 60439

DISTRIBUTION LIST CONTINUED

H. Herman (W-8)
Detroit Diesel Allison-GMC
P.O. Box 894
Indianapolis, IN 46206

M. Herman
Dept. of Materials Science
State Univ. of New York
Stonybrook, NY 11794

Frank Hermanek
Alloy Metals, Inc.
501 Executive Drive
Troy, MI 48084

R. Hillery (M-85)
General Electric Company
MPTL
Cincinnati, OH 45215

J. Stan Hilton
University of Dayton
300 College Park
Dayton, OH 45469

Richard R. Holmes (EH-43)
Marshall Space
Flight Center
Hunstville, AL 35812

Lulu Hsu
Solar Turbines, Inc.
2200 Pacific Highway
San Diego, CA 92138

Larry A. Junod
Allison Gas Turbine Division
P.O. Box 420, Plant 8-T12
Indianapolis, IN 46206

C. Kortovich
TRW Inc.
23355 Euclid Avenue
Cleveland, OH 44117

Propulsion Laboratory (302-2)
U.S. Army Res. & Tech. Lab.
21000 Brookpark Road
Cleveland, OH 44135

Sylvester Lee
AFWAL-MLTM
Wright Patterson AFB
Dayton, OH 45433

A. V. Levy
Lawrence Berkely Lab.
University of California
Berkeley, CA 94720

C. H. Liebert (77-2)
NASA Lewis Research Center
21000 Brookpark Road
Cleveland, OH 44135

E. L. Long, Jr.
Oak Ridge National Lab.
P.O. Box X, Bldg. 4508
Oak Ridge, TN 37831

Frank N. Longo
Metco, Inc.
1101 Prospect Avenue
Westbury, L.I., NY 11590

Richard Martin (9W-61)
Boeing Commercial Airplane Co.
P.O. Box 3707
Seattle, WA 98124

DISTRIBUTION LIST CONTINUED

R. A. Miller (105-1)
NASA Lewis Research Center
21000 Brookpark Road
Cleveland, OH 44135

T. E. Mitchell
Case Western Reserve Univ.
10900 Euclid Avenue
Cleveland, OH 44106

S. Naik
AVCO-Lycoming Division
550 South Main Street
Stratford, CT 06497

J. A. Nesbitt (49-3)
NASA Lewis Research Center
21000 Brookpark Road
Cleveland, OH 44135

J. W. Patten
Cummins Engine Company
Box 3005
Columbus, IN 47202

Ronne D. Proch
Corning Glass Works
31501 Solon Road
Solon, OH 44139

R. J. Quentmeyer (500-220)
NASA Lewis Research Center
21000 Brookpark Road
Cleveland, OH 44135

Gopal Revanton
Deer & Company
3300 River Drive
Moline, IN 61265

David Rigney (D-83)
General Electric Company
Cincinnati, OH 45215

Joseph Scricca
AVCO-Lycoming Division
550 South Main Street
Stratford, CT 06497

Keith Sheffler
Pratt & Whitney Aircraft
400 Main Street
Hartford, CT 06109

T. P. Shyu
Caterpiller Tractor Company
100 N.E. Adams
Peoria, IL 61629

R. W. Soderquist (165-03)
Pratt & Whitney Aircraft
400 Main Street
E. Hartford, CT 06108

D. E. Sokolowski (49-7)
NASA Lewis Research Center
21000 Brookpark Road
Cleveland, OH 44135

C. A. Stearns (106-1)
NASA Lewis Research Center
21000 Brookpark Road
Cleveland, OH 44135

S. Stecura (49-3)
NASA Lewis Research Center
21000 Brookpark Road
Cleveland, OH 44135

DISTRIBUTION LIST CONTINUED

T. E. Strangman
Garrett Turbine Engine Co.
111 South 24th Street
Phoenix, AZ 85034

T. N. Strom (23-2)
NASA Lewis Research Center
21000 Brookpark Road
Cleveland, OH 44135

T. A. Taylor
Linde Division
Union Carbide Corporation
Indianapolis, IN 46224

Robert P. Tolokan
Brunswick Corporation
2000 Brunswick Lane
DeLand, FL 32724

F. C. Toriz
Rolls Royce, Inc.
1985 Phoenix Blvd.
Atlanta, GA 30349

Donald Whicker
GM Research Laboratory
GM Technical Center
Warren, MI 48090

Frank Priest
Chromalloy R&T
Chromalloy Amer. Corp.
Orangeburg, NY 10962

I. Zaplatynsky (106-1)
NASA Lewis Research Center
21000 Brookpark Road
Cleveland, OH 44135